An integrated geochemical and sedimentological analysis of a lacustrine Lagerstätten in the Triassic Cow Branch Formation of the Dan River Basin

Samantha Rose Ritzer

Thesis submitted to the faculty of the Virginia Polytechnic Institute and State University in partial fulfillment of the requirements for the degree of

Master of Science
In
Geology

B. Gill, Committee Chair
B. Romans
K. Eriksson
J. Beard

May 3, 2016
Blacksburg, VA

Keywords: Triassic, Lagerstätte, Iron Speciation, Rift Basin, Anoxia, Sedimentology, Geochemistry

An integrated geochemical and sedimentological analysis of a lacustrine Lagerstätten in the Triassic Cow Branch Formation of the Dan River Basin

Samantha Rose Ritzer

ABSTRACT

The Triassic Cow Branch Formation of the Dan River Basin is host to a world-class lagerstätte deposit of exceptionally preserved insects, among other organisms. The lagerstätte occurs within a cyclic, lacustrine sedimentary succession, hypothesized to have been driven by Milankovitch climate forcing. Through an integrated sedimentological and geochemical investigation, I present evidence that the lagerstätte was deposited during a lake transgression, under intermittently anoxic and ferruginous conditions. Sedimentological evidence shows a deepening followed by shoaling through a broad fining and subsequent coarsening of the sedimentary units of the sequence. This transition in grain size occurs at the lagerstätte. Despite relatively quartz-rich sediments sourced to the basin, silica-content in the studied cycle is exceptionally low. The replacement of silica by the zeolite mineral analcime, coupled with primary dolomite precipitation suggests alkaline lake water. Geochemical evidence, including total organic carbon (TOC), pyrite sulfur and iron speciation data suggest anoxic, ferruginous waters. At the lagerstätte interval, TOC content increases significantly, coinciding with the presence of darker, more laminated sedimentary lithofacies. At the interval of the highest TOC content, a spike in pyrite sulfur content occurs; likely the result of slowed sedimentation. Organic carbon-to-pyrite sulfur ratios suggest however, that the lake water was sulfate-poor and the deep waters never became euxinic (anoxic, H_2S-containing). Iron proxy data show that the studied portion of the Cow Branch Formation deposited under intermittent to persistent

anoxic conditions. These data suggest a confluence of factors — lake transgression, combined with alkaline and anoxic, ferruginous water chemistry — created an ideal scenario that led to lagerstätte formation

Table of Contents:

Dedication

I would like to dedicate this thesis to Dr. John Taylor.
Thank you for noticing my interest in Geo 101 and making it a point to gently nudge me toward changing my major. You hooked me with your genuine love for geology and teaching. Without that, I don't think I would have ever wandered back to science. Whether you realize it or not, you changed the course of my life to pursue a subject that never feels like work. Enjoy your retirement, you deserve it!

Acknowledgements:

I've had a lot of help on this thesis over the last two years.

I would first like to thank my committee for their helpful comments and discussion. I would especially like to thank my committee chair, Ben, for being the best advisor I could have ever asked for. Your understanding of the fact that sometimes life happens combined with the gentle prodding required to get me to write anything down has shaped me as a scientist and a person in the best way possible. Thanks for being both an advisor and a great friend.

I would like to acknowledge the huge help that Scott Traenkner from the Eden Quarry was. Thank you for your genuine interest in the science we were doing, for the giant water trucks, and for access to the quarry. I would also like to thank the Virginia Museum of Natural History, for allowing me to help excavate the insect layer and not getting too mad when I drilled a hole right through it.

I want to thank Paul Olsen for helpful discussion and sharing his years of expertise on the study area.

Thank you Seddies, for distraction at the right times and support through the rest. Matt – you're a great labmate and an even better friend. I'm looking forward to the opportunity to share science and stories with you in the future. Sarah – I probably would have crumbled in the office (and on lime duty) without you, thanks for being a great friend and a person to talk to about rocks and life. I'll miss you buddies!

I'd also like to thank my family, who thinks I'm the smartest person ever, even though they've all seen me struggle with simple math. Your support has been so important and I'd be lost without it. I'd also like to take this time to formally apologize for all of the family gatherings I've missed because of school.

A big thanks to Krista, my best friend and soon-to-be Dr., go us! Your support over the last two years, and the 17 or so before that, has helped me through some of the toughest times I've ever experienced, especially this last year. Cheers to best friendship forever.

Last but not least, Brandon. You are, and always have been, my biggest cheerleader. You deserve this degree as much as I do; putting up with my stress and my tears but always reminding me that I could and would pull this off. The last two years apart have been some of the toughest, but you've been there no matter what. I can't wait to see what rocks the rest of life has in store for our mantle. I love you!

Adios, Blacksburg, I'll miss you. But as Biggie said best, I'm going, going back, back to Cali, Cali!

A. Introduction

A world-class deposit of exceptionally preserved soft-tissue parts of organisms, a Konservat-Lagerstätten, exists in the lacustrine Cow Branch Formation of the Dan River Basin of southern Virginia and northern North Carolina (Figure 1A) (Kent and Olsen, 1997; Olsen et al., 1991). This Triassic deposit contains an assemblage of exceptionally preserved insects, as well as aquatic vertebrates and plant remains from a lake that once existed in the Dan River Basin (Fraser et al., 1996). The insect fossils occur as silvery carbonaceous compressions, preserving micrometer scale morphological detail, on the bedding planes of a dolomitic, microlaminated black shale of the upper Cow Branch Formation. Sedimentary layers immediately above and below the insect layer contain a variety of vertebrates (reptiles and fish), arthropods (shrimp), and plant fossils. Despite nearly four decades of research, geochemical and sedimentological conditions surrounding the deposition and preservation of the Triassic Lagerstätte, including water chemistry and depth of deposition, are still contentious. Here, I present a study to integrate fine scale chemical and sedimentary changes across one climate cycle, including the Lagerstätte, to investigate the environmental setting of this fossil deposit.

1. Geologic Setting

The Dan River Basin — also known as the Danville-Dan River Basin — is one of thirteen Newark Supergroup Basins that formed in the middle to late Triassic during the rifting of Pangaea. Structurally, these basins consist of an asymmetrical-half graben (McBride, 1991 and references therein). Specifically, in the Dan River Basin the Chatham fault zone borders the basin on the northwest and dips to the southeast creating the northeast-southwest

trend of the basin (Ackerman et al., 2003). In the early Jurassic, after sedimentary infill, the basin experienced inversion, probably a result of change in principal stress direction at the onset of central Atlantic seafloor spreading and the emplacement of diabase dikes as a result of CAMP (Central Atlantic Magmatic Province) (Withjack et al., 1998).

The Newark Supergroup collectively describes the continental sedimentary sequences of late Triassic and early Jurassic age found in the North American East Coast rift basins (Froelich and Olsen, 1983). During deposition of Newark Supergroup, the Dan River Basin was located in the tropics close to the equator (Kent and Olsen, 1997). Water and sediment flow into and through the North American rift basins was likely persistent, connecting some basins hydrologically, however none of these basins ever opened enough to introduce a marine component (Leleu et al., 2016). Each basin generally contains basal fluvial sedimentary units, with some basins also containing a fluvio-lacustrine unit (Leleu et al., 2016). The succession of formations in the Dan River Basin consist of, in ascending order, the Pine Hall, Walnut Cove, Dry Fork, Cow Branch and Stoneville Formations (Figure 1B). The units, like those of the Newark Supergroup elsewhere, are primarily comprised of fluvial and lacustrine facies (Smoot, 1991). For this study I have focused on the fluvial Dry Fork Formation and the lacustrine Cow Branch Formation.

Detailed investigation of the magnetostratigraphy of the Dry Fork-Cow Branch succession has allowed for it to be correlated to a geomagnetic polarity sequence from the Newark Basin (Kent and Olsen, 1997; Olsen et al., 2015). This correlation suggests that deposition of the Dry Fork and Cow Branch Formations occurred during the Norian Stage of the Late

Triassic with deposition spanning 224 Ma to 216.5 Ma (Kent and Olsen, 1997; Olsen et al., 2015).

The Cow Branch Formation, which hosts the insect lagerstätte, consists of primarily lacustrine facies and is approximately 1900 meters thick near the basin depocenter (Van Houten, 1962). The best exposure of this unit is found in the Eden Quarry, which is located on the Virginia-North Carolina State Line (Figure 1A). Lacustrine lithofacies of the Cow Branch display cyclicity consisting of 8-11 meter packages which contain organic-rich shale that generally grades into siltstones and sandstones that contain mudcracks and ripple cross bedding (Olsen, 1986; Smoot, 1991). These cyclic facies packages, termed Van Houten cycles, have been related to astronomical forcings on the climate on the 21,000 year precessional timescales that controlled the water balance of the lake (Olsen, 1986). While the cyclicity of the lacustrine facies has been suggested to be driven by climate cycles (evaporation vs. precipitation) (Olsen, 1986), the transition from fluvial to lacustrine facies likely was also influenced by other factors including the topography of the sediment source area and changing gradients of tributary streams, and sedimentary accretion within the basin (Leleu et al., 2016; Smoot, 1991).

The Dry Fork Formation is found both below and interfingers laterally with the Cow Branch Formation (Olsen et al., 2015; Smoot, 1991). Once considered a transition between the coarser, fluvial Pine Hall and the more fine-grained, lacustrine Cow Branch Formation, the Dry Fork is now considered to be a marginal fluvial facies (Olsen et al., 2015). The Dry Fork Formation consists predominantly of red to purple, fine-grained, cross-bedded

sandstone, siltstones, and mudstones with less frequent lenses of finer, dark grey lenses of mudstone (Olsen et al., 2015). Here we use the geochemistry of the lithofacies from the marginal Dry Fork Formation to compare to those in the lacustrine Cow Branch Formation that were deposited towards the basin depocenter in order to determine paleolake chemistry and relative depth of deposition of the insect lagerstätte.

2. Van Houten Cycles in the context of the Cow Branch Fm.

As noted above, the cyclic facies of the Newark Supergroup, termed Van Houten cycles have been linked astronomical forcings on the climate on the 21,000 year, precessional, timescales (Olsen, 1986). In stratigraphic ascent, the classic Van Houten cycle, as originally defined in the Newark Basin, begins with a relatively coarse red sandstone, often containing reptile trace fossils and well-preserved flora, which are suggestive of a shallow, playa-like lake environment. This red sandstone grades into fine sandstones and siltstones with a purple color, containing similar fossils. These two facies have been defined as Division 1 by Olsen et a. (1986), and are suggested to represent units deposited during a lake level rise. This division is present in the Cow Branch Formation, however only cross-bedded light grey, fine-grained sandstones are present within the cycle that contains the lagerstätten. More ideal division 1 units, including coarse grained, red sandstones with dessication features can be found elsewhere in the Cow Branch Formation. Above the purple clastic units the cycle tends towards smaller grain sizes, including grey siltstone intervals topped with dark grey to black mudrocks, containing aquatic vertebrate fossils such as fish and the aquatic reptile *Tanytrachelos*, as well as an exceptionally well-preserved flora. In the Eden Quarry this unit also contains the insect lagerstätten. These

facies have been defined by Olsen et al. (1986) as division 2 and represent a lake high-stand. Moving further up within the cycle, the units tend back towards the grey siltstones and purple and red coarser-grained facies, defined as division 3 that represents a lake-level fall (Olsen, 1986). As described previously in Division 1, the grey siltstone to fine sandstone facies characterize the beginning and end of the cycle investigated in this study (Figure 2).

In addition to the lithological changes associated with Van Houten Cycles, Olsen (1986 and 1989), noted several geochemical trends within these cycles. In the two studied cycles from the Cow Branch Formation, carbonate content steadily decreases up section from the laminated claystone facies (division 2; defined by Olsen, 1986) and only increases once again with the next stratigraphic appearance of division 2 facies. There is also a short interval of increased sulfur content at the initial transition to division 2 facies (Olsen 1986; Olsen et al., 1989). The sulfur content throughout the cycles investigated never exceeds 1 wt % with an average abundance of 0.2 wt%. Also within the laminated claystone facies of the Cow Branch formation cycles, there is an increase in total organic carbon abundance from a baseline of 0.5-1.0 wt % to nearly 4.0 wt% (Olsen, 1986; Olsen et al., 1989).

Several lines of evidence suggest the lake was alkaline. Despite an abundance of quartz in the shallow facies of Dan River Basin (Thayer et al. 1970) there is substantially less preserved within the cycle containing the lagerstätten and the Cow Branch Formation as a whole. Instead, there is an abundance of analcime, a zeolite (a sodium aluminum tectosilicate mineral) commonly found in alkaline lakes (Hay, 1966) is present as a coarser component, generally coarse sand and larger. Given the differing chemical stabilities of analcime and quartz with pH, the mineralogy suggests that the lake chemistry was alkaline. This is further supported by the presence of microsparry dolomite, which is present

throughout the cycle containing the lagerstätten (Liutkus et al., 2014; 2010). Dolomite is known to precipitate in some alkaline lakes at pH values greater than 9 (Casado et al., 2014), also suggesting that the Dan River lake was alkaline.

3. Models for the environment of formation of the lagerstätten

There are currently two competing hypotheses for the environment of preservation of the Konservat-Lagerstätten at the Virginia Solite Quarry. Olsen et al., (2015, 1978) propose that the preservation is a result of deposition of the fossils in a perennially chemically stratified lake. They suggest that the anoxic environment below the chemocline in the lake inhibited the scavenging and slowed microbial breakdown of the fossils. The initial transgression of anoxic waters over more shallow sediments near the lake margins would have allowed for the preservation of the soft tissue of the deposited organism (Olsen et al., 2015).

Like Olsen (1978), Litkus et al., (2010) suggest the preservation of the lagerstätte is also product of a lake transgression. However in contrast, they suggest the environment of preservation was a shallow, alkaline lake environment influenced by the chemistry of groundwater seeps at the lake margins. In their model, Liutkus et al. (2010) note that the deepest water, finely laminated, organic carbon-rich facies occur above the layer hosting the insect lagerstätten. They cite occurrences of primary dolomite and analcime, as well as the enrichment of F, Ca and Mg in the strata around the insect layer and the insect layer itself as evidence of alkaline and potentially toxic waters that limited inhibited the scavenging of the insects.

With the geochemical and sedimentological evidence presented here, I will thest the two models. In a more basinward environment, as the Olsen (2015; 1978) hypothesis suggests,

data will show an active iron shuttle in the presence of anoxia, reflected as an enrichment in highly reactive iron and increased organic carbon contents. In a more marginal and alkaline environment as Liutkus et al. (2010) suggests, alkaline minerals will be present in conjunction with variable organic carbon isotope values and little to no enrichment in highly-reactive iron.

B. Methods

1. Core acquisition and sampling

Three 4 cm diameter cores totaling approximately 11 meters of material were taken from Cow Branch Formation at Eden Quarry (36.540782°N, 79.672190°W; Figure 1A) using a Shaw Backpack Drill. These cores sampled the sedimentary cycle that contains the insect lagerstätte and part of the underlying cycle. The first core, Q1Pt, captured the 4.5 meters of stratigraphy that included the lowest part of the cycle, including the horizon that contains the insect lagerstätten, and the upper portion of the cycle below it. This core was drilled into the exposed face previously excavated by the Virginia Museum of Natural History during their excavation of the insect lagerstätten. Core Q1Md, captured the 3 meters of the middle portion of the lagerstätte cycle and was drilled into an exposed face, approximately 9 meters from Q1Pt. Core Q1Br captured 4 meters of the upper portion of the cycle, was drilled on the bench above the two exposed faces. It was drilled 5 meters from Q1Pt, on the same line, perpendicular to strike. In total, these three cores sampled 11 meters of nearly continuous stratigraphy. The two lower cores (Q1Pt and Q1Md) were correlated via a set of fine-grained massive siltstone beds at 275 cm in the lower composite section (Figure 3). Henceforth, the correlated core sections Q1Pt and Q1Md will be referred to as "Bottom Core" and core section Q1Br will be referred to as "Top Core."

After collection, the core material was cleaned and slabbed with a water-cooled rock saw. The slabbed cores were then logged and described at the mm to cm scale, noting lithology and mineralogy, color, sedimentary structures, trace fossils and bioturbation, and grain size. Ultimately 33 intervals were selected for thin sections that were representative of

major facies and sedimentary structures. The cores were also sampled approximately every 25 cm for geochemical analyses. The sample powders were obtained using a Dremel tool with a diamond bit and homogenized using a mortar and pestle. Care was taken to avoid sampling weathered portions of the cores and intervals with secondary veins, as well as an observed fault zone. In total, 40 samples representative of facies and compositions were selected for geochemical analysis.

Eleven hand samples from the fluvial Dry Fork formation were also collected from exposures along Dry Creek, a tributary of the Dan River that flows through Eden, North Carolina (36.488362°N, 79.758821°). The samples were collected from a ~225 m transect along the bank of the creek and their stratigraphic order was noted, but distance from one another stratigraphically was not logged. The Dry Fork hand samples were also sampled via a Dremel tool and the resulting powders were homogenized.

2. Total organic carbon (TOC) contents and isotope compositions ($\delta^{13}C_{org}$)

Samples were acidified with 2N HCl for 24 hours to remove carbonate carbon from the sample. The samples were then rinsed with doubly deionized (18 mΩ□□water until the pH of the solution overlying the sample was neutral. Samples were then dried and loaded into tin capsules for analysis. Determination of total organic carbon (TOC) contents and isotope compositions were conducted on an Isoprime 100 continuous flow isotope ratio mass spectrometer interfaced with an Elementar vario ISOTOPE elemental analyzer. Precision of carbon content analyses was determined by replicate of samples and commercial elemental standards were equal to or better than 0.1 wt % (1□). All carbon isotope compositions are

reported in standard delta notation as per mil (‰) deviations from Vienna Pee Dee Belemnite (V-PDB):

$\delta^{13}C = (((^{13}C/^{12}C_{sample})/(^{13}C/^{12}C_{VPDB})-1)*1000$

Replicate analyses of samples and international standards (IAEA CH-6 and CH-7 and commercial standards) were equal to or better than 0.1‰ (1σ).

3. Iron speciation analyses

Iron speciation analyses are used here to evaluate redox conditions within the lake (Poulton and Canfield, 2005). Iron is soluble and mobile in the Fe(II) valence state under anoxic conditions, but readily forms oxide and hydroxide minerals and is thus immobile when in the Fe(III) valence state under oxic conditions. Iron bound in minerals that are reactive towards aqueous sulfide and will form pyrite during early diagenesis are termed part of a pool termed highly reactive iron (Fe_{HR}). This includes iron found in carbonates, iron hydroxides and oxyhydroxides, magnetite, as well as, in pyrite itself (Poulton and Canfield, 2005; Canfield et al., 1986; 1996; Anderson and Raiswell, 2004). Remainder of the sedimentary iron not found in the highly reactive is termed the unreactive iron pool (Fe_U) and is predominately consists of silicate bound iron.

Samples were subjected to a sequential procedure that extracts iron from different operationally defined, mineralogical pools in the sample following the procedures of Poulton and Canfield (2005). Briefly, this sequential extraction consisted of: 1.) 1 M sodium acetate heated at 50°C for 48 hours to extract iron from carbonate minerals (Fe_{carb}) siderite and ankerite; 2.) sodium dithionite (50 g L^{-1}) for 24 hours to extract iron from oxides and

hydroxides (Fe_{ox}); and 3.) 0.2 M ammonium oxalate and 0.17 M oxalic acid for 6 hours to extract iron from magnetite (Fe_{mag}).

After each extraction, an aliquot of the solution was taken for determination of its iron contents. Iron contents of the solutions were determined via the ferrozine spectrophotometer method (Stookey, 1970; Viollier et al., 2000) Replicate analyses of samples using this method yielded a precision of 0.03% (1σ).

4. Pyrite sulfur and iron contents

Extraction and quantification of pyrite sulfur from the samples was achieved using the chromium reduction method (Canfield et al., 1986). During the extraction, approximately 0.6 g of sample was reacted with 40 mL of 1 M chromous chloride solution and 20 mL of 12 N HCl and heated for two hours in a specialized distillation line under a nitrogen atmosphere. This liberated hydrogen sulfide, which was then reacted in 0.24 M zinc acetate solution recovering the sulfide as ZnS. The ZnS was then converted to Ag_2S with the addition of 0.18 M $AgNO_3$ solution. The Ag_2S precipitate was isolated by filtration (45 μ m) and was dried. Pyrite sulfur concentrations were determined by gravimetry with a precision of ±0.03 wt % (1σ) for repeat analyses. Pyrite iron contents were calculated using the pyrite sulfur contents assuming the stoichiometry of pyrite.

5. Total iron content

The determination of total iron content followed the procedures of (Aller et al., 1986). Samples were initially ashed in a furnace at 900°C for approximately 6 hours. The ashed

samples were then loaded into Savillex vials with 4 mL of 12 N HCl and heated at 150°C for 48 hours. After the reaction, aliquots of the solutions were taken to determine the total iron content via the ferrozine spectrophotometer method (Stookey, 1970; Viollier et al., 2000). Replicate analyses of samples using this method yielded a precision of ±0.02 wt % (1σ).

C. Results

1. Cow Branch lithofacies descriptions

Within the collected cycle, ten different lithofacies have been delineated. Two of the lithofacies have also been divided into sub-lithofacies. I term these lithofacies "microfacies" due to the fact that they are chosen on a cm-scale and can be found in units as thick as 60 cm down to 4 cm. Broadly the lithofacies correlate well with those described by (Smoot, 1991). Smoot (1991) noted that the Dan River Basin contains L1 through L4 lithofacies. In the cycle of study, however, only lithofacies L1 through L3 are present and are described as follows; L1 is described as flat, continuous laminations with some pinch and swell structures, as well as more calcareous intervals. L2 is characteristically bioturbated and massive. L3 indicates current reworking, often having scours and pinch and swell structures. I have noted which of my lithofacies designations are equivalent to those of Smoot (1991) in Table 1. It should also be noted that fractures were present throughout the studied stratigraphy and were generally filled with calcite and minor amounts of iron oxides. Soft sediment deformation and sedimentary dikes several centimeters in diameter were also prevalent throughout the studied section.

i. Lithofacies 1

This lithofacies occurs in two units within the studied section (Figure 3; Table 1). The intervals consist of medium grey shale to fine silt sized dolomite and clay, interbedded with light grey to grey-blue fine to medium siltstone. These beds contain fine to medium siltstones and often include white, relatively coarse (medium sand) grains of analcime. Individual beds are roughly 0.5 to 1 cm thick and the contacts are generally deformed by

soft sediment deformation. Despite this, the contacts between the grey shale to fine silt layers and the grey-blue fine to medium silt layers are sharp (Figure 4.1).

ii. Lithofacies 2a

Nine units consist of this lithofacies within the studied section (Figure 3; Table 1). These intervals comprise of grey shale to very fine siltstone with fine scale (approx. 1-5mm) convoluted interbeds of predominantly clay and dolomite. This lithofacies also contains irregular structures that are generally lighter than the surrounding rock, but do not contain noticeably coarser grains. Throughout the interval exist occasional white (fine to medium sand size) grains, similar to Lithofacies 1. The very top of this lithofacies interval from Bottom Core 110-117 cm displays upward fining. At the stratigraphic top of this small scale fining up sequence there exists a large (approximately 3 mm x 5 mm) dark, angular phosphatic fossil that is much larger than the surrounding grains (Figure 4.2).

iii. Lithofacies 2b

One example of this lithofacies is present within the section (Figure 3; Table 1). This lithofacies consists of lithofacies 2a interbedded with lithofacies 3 at the 1-2 cm scale. The contacts between the two lithofacies types are irregular or appear deformed (Figure 4.3).

iv. Lithofacies 3

This lithofacies is the most predominant within the studied stratigraphic section making up 13 defined units (Figure 3; Table 1). This lithofacies is medium grey in color and is made up of primarily dolomite grains that range in size from clay to fine silt. The units are generally

massive with some occurences of soft sediment deformation, visible with color differences. Typically, intervals associated with these lithofacies have unconformable or erosional surfaces within them. Horizons containing 3-5mm thick accumulations of pyrite also are visible within two units (Figure 4.4.a). The upper of these two intervals also include phosphatic nodules. The interval between 414-448 cm in the top core includes a lighter grey irregular shape similar to those described by (Pratt, 1998; Rodríguez-Pascua et al., 2000; Smoot, 1991), visible by color difference and slight change in grain size, and possibly represents an intrusion of another lithofacies into this lithofacies.

v. Lithofacies 4

This lithofacies occurs only once within the studied section (Figure 3; Table 1), but is the longest continuous lithofacies unit, at nearly 60 cm thick. It is massive, blue/grey in color, and appears to be bioturbated with no apparent grain-size trend. It is composed of very fine silt with a heavy presence of medium sand sized white grains of analcime. This lithofacies also includes medium to coarse silt sized black mineral grains (Figure 4.5).

vi. Lithofacies 5a

There are two occurrences of this lithofacies within the studied section and both are relatively thick units, 22 and 52 cm (Figure 3; Table 1). The units are very dark grey to black shale composed of microsparry dolomite and clay with very fine scale (sub-mm) laminations. Laminations are carbonate rich, predominantly dolomitic and generally lighter than the black shale and are not perfectly straight when viewed in thin section. The core in these intervals is commonly chippy and fragmented. The intervals often contain coprolites

that deform the surrounding beds. White grains of fine sand size analcime are rare, as well as larger, medium-coarse sand sized white nodules that appear to be aggregates of a number of smaller (coarse silt to fine sand size) analcime and other black mineral grains (Figure 4.6). These nodules are unreactive towards HCl. Compressed plant fossils are also occasionally visible parallel to the bedding planes. The higher of the two intervals, Bottom Core 375-427 cm includes bone fragments, as well as, "loop structures". These structures have been interpreted elsewhere as being caused by syndepositional microfaulting that interrupts the fine scale laminations and creating the look of looped lamination structures (Calvo et al., 1998; Rodríguez-Pascua et al., 2000). The Bottom Core interval from 255-277 cm includes the insect layer.

vii. Lithofacies 5b

This lithofacies occurs in 6 intervals within the section (Figure 3; Table 1). Sedimentologically, it is quite similar to lithofacies 5a. However it is slightly coarser grained than lithofacies 5, however the grain sizes are still not silt sized. The color ranges from very dark grey to dark grey with fine scale (sub-mm) wavy laminations similar to those seen in 5a. Compressed plant fossils, preserved as silvery carbon compressions, are visible on bedding planes. Loop structures are observed in most intervals of this lithofacies (Figure 4.7.a). White analcime grains, as described in other lithofacies, are rare but occasionally present, as well as, previously described black grains. The major differences from lithofacies 5a are the slightly coarser grain size and the uncommon occurrence of nodules. The top core interval from 84-130 cm includes a lighter (medium grey) and somewhat coarser (fine silt) structure that appears similar to the one seen in lithofacies 3,

possibly the sedimentary intrusion of a different lithofacies like those described by Pratt, 1998; Rodríguez-Pascua et al., 2000; Smoot, 1991, (Figure 4.7.b).

viii. Lithofacies 6

This lithofacies occurs only once within the studied section (Figure 3; Table 1). It occurs in fault zone and consists of a brecciated black shale with a coal-like texture and contains fractures filled with white calcite veins.

ix. Lithofacies 7

There is one example of this lithofacies within the studied stratigraphy (Figure 3; Table 1). It ranges from a very dark grey to black shale to very fine silt-sized clays and microsparry dolomite with convoluted interbeds on the 2-5mm scale, noted by color change. The lower part of the interval includes mm-scale pyrite nodules, a bone fragment, and unidentifiable compressed fossils. Loop structures also occur, but are often hard to pick out due to the consistent dark of this lithofacies. Occasional white analcime nodules (1-2 mm scale) and grains (< 1mm) described in previous lithofacies are also present.

x. Lithofacies 8

There is one interval of this lithofacies type within the studied section (Figure 3; Table 1). This lithofacies is generally a dark grey shale to very fine silt with mm scale ripple cross-bedding (Figure 4.8). The intervals are otherwise very similar to lithofacies 7.

xi. Lithofacies 9

This lithofacies comprises small (1-2mm) massive dark brown beds of fine silt that occur in four isolated intervals within the core cycle (Figure 3; Table 1). While these units are an order of magnitude smaller in scale as compared to units of the other lithofacies they are distinct and make unique marker beds that were used to correlate the Bottom Core composite section (Figure 4.9).

xii. Lithofacies 10a

There are four intervals of this lithofacies within the core cycle (Figure 3; Table 1). These are predominantly comprised of massive, weathered units that range from medium brown to rust orange to light orange in color. Grain size ranges from very fine silt to fine sand. Fine sand intervals may be a product of dissolution of smaller grains and give the appearance of a larger grain size. I note this lithofacies separately because of its weathered nature and, likely had they not been exposed to weathered, they may have fit into another lithofacies designation (Figure 4.10).

xiii. Lithofacies 10b

There are two instances of this lithofacies within the core (Figure 3; Table 1). The intervals are essentially the same as lithofacies 10 with respect to grain size and color, however faint, fine scale (sub mm) laminations can be observed (Figure 4.11).

2. Dry Fork lithofacies descriptions

A detailed lithofacies analysis was not conducted on the samples from the Dry Fork Formation. Hand samples collected from the Dry Fork range from red to orange brown, massive coarse siltstones to very fine-grained sandstones. The Dry Fork interval from which we sampled probably resides in F4 or F5 as defined by Smoot (1991). F4 includes fining up sequences of sandstone to silty mudstone and F5 are inclined beds of fine sandstone to mudstone, with mud being deposited during slack periods (Smoot, 1991).

3. Interpretation of depositional processes

Broadly, lithofacies can be divided into two main groups. Lithofacies 1-4 and 8 are interpreted as having been deposited in a more marginal environment. While grain size throughout the cycle remains relatively small, the coarsest grain sizes (medium-coarse silt and fine sand) are seen in these lithofacies. Smaller-scale transitions can be seen in lithofacies 3, suggesting a more shallow and dynamic depositional environment. Structures throughout these lithofacies are also indicative of a more marginal environment, including heavily bioturbated intervals like lithofacies 4, as well as ripple structures in lithofacies 8, indicating reworking of sediment by currents. As a group, these lithofacies exhibit a broad fining-up trend in the bottom of the core, indicating deepening, and a coarsening-up trend in the top of the core, indicating shoaling. The second lithofacies group, lithofacies 5-7 separates the two grain-size trends as the more basinward depositional environment.

As previously stated, lithofacies 5-7 are interpreted to have been deposited in a more basinward position. Evidence for this interpretation includes visible darkening of the lithofacies, suggesting increased organic carbon content as well as presence of the finest

grains (clay to very fine silt size) within the cycle. Structures indicative of deposition in low energy environments, such as fine-scale laminations and microbial mat-like structures are present in all lithofacies within this group. The lack of any grain size trend suggests that these lithofacies were deposited within a lake high-stand, potentially distally enough that higher-order fluctuations in lake level or accommodation were not recorded as lithofacies changes.

Lithofacies 9 is interpreted as having been deposited in a more marginal environment with conditions favoring primary carbonate precipitation, as beds are thin but massive and almost entirely dolomitic. This lithofacies was distinguished from the other marginal lithofacies due to its use as a marker bed for correlation between core Q1Pt and core Q1Md to form the composite "bottom core."

Lithofacies 10a and 10b are separated from the marginal lithofacies group due to their weathered nature. Remnant structures present within the lithofacies, such as ripple cross-bedding and potential fluid escape structures suggest that if not for their weathering, they would be included in the marginal lithofacies group.

4. Geochemistry of Cow Branch Samples

i. Total organic content and C_{org} isotopes

Stratigraphic trends of total organic carbon contents follow lithofacies changes to a high degree. Low TOC (0.25-0.5 wt%) contents occur in the lighter, more coarse-grained lithofacies (1-4) with few exceptions. Towards the middle of the core cycle with the first transition into lithofacies 5a, the TOC rises sharply. Over approximately the next 60 cm, the color of the lithofacies rapidly change from grey to dark grey to black and the color change

coincides with the rise in TOC from ~0.25 wt% to a peak abundance of 3.5 wt%. The insect lagerstätte occurs in the early part of the lowest unit of lithofacies 5a (from Bottom Core 255-274) in this interval of increasing TOC contents. It is also noteworthy that the highest TOC values occur in the darkest colored, finely laminated lithofacies (5a and b) (Figure 3).

These high TOC levels are sustained through the interval comprised of lithofacies 5-7. TOC contents begin to decline up section with the transition back to intervals of lithofacies 1-4. Towards the top of the cycle, around Top Core 285 cm in the last appearance of lithofacies 5b, the color is less dark than similar stratigraphically lower units, but TOC is still increased above background at 1.5 wt % (Figure 3).

Organic carbon isotopes isotope values through the entire studied section range from approximately -29‰ to -22‰. Carbon isotope values tend to be the most negative in lithofacies 5-7 and have relatively narrow range isotope compositions; -29‰ to -27.5‰ with a few outliers. Conversely, organic carbon isotope compositions of lithofacies 1-4 show a broader range of compositions -27.5‰ to -21.7‰ (Figure 3).

ii. Pyrite sulfur content

Overall pyrite sulfur contents are low for the entirety of the cycle with the highest content reaching 0.39 wt % sulfur. However there is there is an increase in pyrite sulfur that coincides with the increase in TOC and first instance of lithofacies 5a. However, unlike the TOC values, the sulfur content does not stay consistently high throughout the middle

section of the sedimentary cycle and rapidly decreases up section as you move out of lithofacies 5a.

iii. Iron speciation

Iron speciation, as described in the methods section, was used to determine the mineralogical pools where iron is bound. Four separate pools were determined; carbonate iron (Fe_{CARB}), iron (oxy)hydroxides (Fe_{OX}), magnetite (Fe_{MAG}), and pyrite iron (Fe_{PY}) (Figure 5). Carbonate-bound iron (Fe_{CARB}) was generally the most abundant and highly reactive iron pool throughout the studied interval ranging from 1 to 1.3 wt%. This pool of iron tended to compose 20% to 25% of the total iron pool. Iron bound in (oxy)hydroxides (Fe_{OX}) do not make up an appreciable part of the total iron pool throughout the entire cycle with values of less than <1 wt%, and make up typically between 3 to 6% of the total iron pool. Oxy-hydroxide bound iron content does not correlate with any lithofacies type but did become slightly more abundant in lithofacies adjacent to the weathered lithofacies (weathered intervals within the core cycle were not sampled for geochemistry.).

Magnetite iron (Fe_{MAG}) is present in all of the core samples and tends to be the second most abundant iron pool within the highly reactive iron pool. Fe_{MAG} values do not follow any clear trends stratigraphically, but in many cases is more abundant when Fe_{CARB} is less abundant. Magnetite makes up approximately 5 to 10% of the total iron. Compared to the entire sample, magnetite makes up about 0.4 to 0.6 wt% with some exceptions in both directions.

Iron bound in pyrite or sulfide minerals (Fe_{PY}) is sparse throughout the entire core cycle. Values are notably low, with Fe_{PY} making up less than 4.5% of the total iron. Fe_{PY} never

exceeds 0.35 wt % of the total sample and is generally around 0.05 wt% or less. However, in samples that coincide with higher TOC contents and more negative $\delta^{13}C_{org}$ like lithofacies 5-7, Fe_{PY} contents range from 7.1 to 9.6% of the total iron. Though pyrite lags were avoided while sampling, higher Fe_{PY} values do occur with lithofacies 3 that contain these lags (Figure 3).

Geochemistry of the Dry Fork Samples

i. Total organic content and C_{org} isotopes

TOC contents for the Dry Fork samples low. Samples collected range in value from 0.04 to 0.07 wt% TOC. Through the stratigraphic progression of the sample set, there are no visible trends. The TOC contents were also marginally lower than lowest content seen in the Cow Branch samples. $\delta^{13}C_{org}$ values for the Dry Fork samples were range from -26.72‰ to -28.16‰. Compared to the core values, the Dry Fork lithofacies are closer to the values of Cow Branch Formation lithofacies 5-7 as described above, but are slightly less negative by ~1‰ (Figure 3).

ii. Iron speciation:

The Dry Fork samples are generally low in Fe_{CARB} and on average is less than 0.25 wt% of the total sample and it makes up from 1 to 5% of the total iron pool. Fe_{CARB} abundance is also an order of magnitude less than those of the Cow Branch. The Dry Fork samples are appreciably lower than the Cow Branch in Fe_{MAG} as well, with all values less than 0.17 wt % of the total sample and making up less than 2.7% of the total iron pool. Fe_{PY} in the Dry Fork samples matches the lowest values in the Cow Branch formation (lithofacies 1, 2, 4 and 5b),

roughly 0.00 to 0.05 wt % of the total sample and less than 0.7% of the total iron pool. However, Fe_{OX} is more abundant compared to the Cow Branch samples, ranging from 0.53 to 0.80 wt % of the total sample and 11 to 16% of the total iron pool (Figure 5).

D. Discussion

1. Lithofacies succession and lake level history

To a large degree, the lithofacies data observed within the stratigraphic cycle collected agrees with the previously investigations of the Cow Branch Formation (Smoot, 1991; Olsen, 1986; Olsen et al., 1989; 2015; Van Houten, 1962; 1964). There is a notable stratigraphic progression of lithofacies that suggests a deepening and subsequent shoaling of the local lake environment. Lithofacies 1-4 make up the majority of the lower half of the cycle. Lithofacies 1 and 2 are among the coarsest in the cycle with silt-sized grains. Lithofacies 3 is the most common lithofacies in the cycle with respect to both stratigraphic range and combined thickness of constituent packages. Its massive structure, intermediate grain size (clay size to fine silt) and stratigraphic position may suggest this is a transitional lithofacies between intervals dominated by lithofacies 1 and 2 and lithofacies 4. The fine-grained matrix (with the exception of coarse silt to sand sized secondary grains) of lithofacies 4 is massive, like lithofacies 3, suggesting that it is heavily bioturbated and would then represent an environment conducive for benthic organisms to inhabit the lake floor.

Within the lower half of the studied section there is a general up-section fining of grain sizes. This portion of the section can be divided in lithofacies packages that also fine upward: Lithofacies 1-2a transitioning into lithofacies 3. This pattern suggests high

frequency transgressive cycles that were the product of changes in lake level during this interval.

Continuing up-section there is the relatively abrupt appearance of lithofacies (5-7) that consist of darker, finer-grained lithologies, predominantly shales. These units have been traditionally interpreted as deep water lithofacies (depth rank 4-6 of Olsen et al. 1986) and their initial stratigraphic appearance with little to no interfingering (although lithofacies 2b could be considered the transition interval) suggests a local deepening of the environment and marks a transgressive interval of the cycle followed by a lake highstand. Notably, the insect lagerstätte occurs in this initial transgressive interval. Further evidence for lake transgression is the short-lived relative enrichment in pyrite. This may be reflective of slowed sedimentation rates compared to the rest of the cycle as a whole, which allowed for a greater amount of authigenic pyrite formation.

I consider both subsets of lithofacies 5 to be deposited in a relatively deep environment given the high TOC contents, preserved lamination and lack of bioturbation and lack of current produced sedimentary structures. However there is a notable distinction between the two subfacies of lithofacies 5 that may reflect changes within the lake environment:

a. Lithofacies 5a contains a greater abundance of larger secondary analcime grains, which signals that the lake water or pore waters within the sediments were saturated with respect to this mineral. This may reflect a higher salinity (and greater contents of Ca and Mg) of the lake water during the deposition of this lithofacies.

b. Lithofacies 5b is essentially the same lithofacies as 5a, but the most striking difference is the lack of large analcime grains and nodules. This could be because 5b represents sediments deposited at lake high-stand, where the lake waters were freshest and/or the supply of clastic silicate minerals or volcanic glass (that would have supplied silica for the production of analcime) to the central part of the basin was decreased. Both of these factors would have resulted in an overall decline in analcime saturation.

Continuing up-section, with the stratigraphically highest instances of the more basinward lithofacies 5b, lithofacies 3 begins to reappear and above which coarser grain lithofacies once again begin to dominate the cycle. Within the upper half of the cycle there is a general up-section coarsening of grain sizes. The lithofacies in this portion of the section can also be divided in lithofacies packages that also coarsen upwards: Lithofacies 5b transitioning into lithofacies 3 to 2a. This pattern is suggestive of higher frequency regressive cycles within this interval.

While lithofacies 10a and 10b are designated as separate lithofacies due to their weathered nature, it is likely, based on the few sedimentary structures preserved and their stratigraphic position, that they would have originally represented lithofacies divisions 1, 2 and 3.

In summary, over the studied stratigraphic interval the lithofacies changes are interpreted to show a gradual deepening and subsequent shallowing of the local lake environment. Olsen (1986) and Olsen et al. (1989) linked the lithofacies changes on this scale to the 21

kyr precessional cycle using power spectra analysis of the thickness of lithofacies units classified with their depth rank classification. It is also notable that superimposed on this broader change, there are clear higher order cycles that likely reflect shorter-term changes in lake level.

2. Iron shuttle model and sedimentary redox in the Dan River Basin

In modern anoxic basins like the Black Sea, there exists an active iron shuttle that enriches the deep basinal sediments in highly reactive iron relative that shallow shelf sediments deposited under oxic to suboxic waters (Raiswell and Canfield, 1998; Anderson and Raiswell, 2004; Poulton and Raiswell, 2002; Lyons and Severmann, 2006). In the oxic waters, iron is generally found as ferric iron, Fe (III), and is immobile and insoluble, precipitating as iron oxide and hydroxide minerals. However, when these ferric iron minerals are buried in shallow reducing sediments on the margins of an anoxic basin, they can be subsequently reduced to ferrous iron, Fe(II) and released back into the water column. This iron can then undergo a repetitive cycle of oxidation and reduction, with Fe(II) in solution being reoxidized and redeposited back into the shelf sediments as iron (oxy)hydroxide minerals. However some of the Fe(II) remains in solution and can be eventually transported or 'shuttled' from the margin to the anoxic water column above the deep basin. Without the capacity to become oxidized again, the iron eventually precipitates as ferrous iron bearing minerals that are deposited in the deep basin sediments (Canfield et al., 1996; Raiswell and Canfield, 1998; Anderson and Raiswell, 2004; Lyons and Severmann, 2006). This overall process causes an enrichment of highly reactive iron over the total iron (reflected in the ratio: Fe_{HR}/Fe_{TOT}) in the deep basinal sediments as compared to the

shallow shelf sediments (Anderson and Raiswell, 2004; Canfield et al., 1996; Poulton and Raiswell, 2002; Raiswell and Anderson, 2005). Hence this proxy can be used to identify the presence of anoxic water columns in ancient settings (Figure 6).

This proxy has been most often applied to both modern and ancient marine basins, where oxic sediment baseline values can or have been established (Canfield et al., 2008; Farrell et al., 2013; Lyons and Severmann, 2006; Raiswell et al., 2011, 2001) However, in order for this proxy to be applied in my study of the Dan River Basin, the Fe_{HR}/Fe_{TOT} of the oxic environments that were the source of iron to the deep basin must be identified. In the case of the Dan River Basin, I have utilized the fluvial Dry Fork Formation — the formation directly underlies and is also laterally equivalent to the Cow Branch Formation (see "Lithofacies Descriptions" above) — to establish oxic Fe_{HR}/Fe_{TOT} baseline for the Dan River Basin (see oxic Figure 3).

The iron speciation data from the Cow Branch and Dry Fork Formations suggests that an iron shuttle was active during the deposition of the studied section of the Cow Branch Formation (Figures 2, 4, and 5). Throughout the section highly reactive iron is consistently enriched in highly reactive iron over total ($Fe_{HR}/Fe_T \approx 0.40$) as compared to the samples from Dry Fork Formation ($Fe_{HR}/Fe_T \approx 0.20$) (Figure 3). However, it is important to note here that samples from Dry Fork Formation are not time equivalent to the Cow Branch Formation as they are from the portion of the Dry Fork Formation that underlies the Cow Branch; samples from what would be the time equivalent Dry Fork Formation were not available to be sampled. However based on the consistency of the Fe_{HR}/Fe_T from Dry Fork Formation over ~150 meters of the sampled stratigraphy and the large enrichment found

in the Cow Branch Formation suggests they are valid for establish the oxic baseline values for the basin.

Thus based on this data, the studied sequence of the Cow Branch Formation was deposited under anoxic waters, based on the enrichment of the highly reactive iron over that seen Dry Fork Formation (Figure 3). Also, based on the proportion of pyrite bound iron to total highly reactive iron (Fe_{py}/FE_{HR}), data suggest that water column was never euxinic (anoxic and H_2S-rich). In modern systems deposited under euxinic conditions, Fe_{py}/Fe_{HR} exceeds 0.75, that is 75% of the highly reactive iron pool is found in pyrite (Raiswell et al., 1988). Any instances of increased pyrite iron content appear to coincide with intervals of either low sedimentation rates like lithofacies 5a and 5b or pyrite lags near unconformable surfaces like those observed lithofacies 3 that likely accumulated by reworking and winnowing of sediments.

By comparing organic carbon to the pyrite sulfur contents of the Cow Branch samples, it is clear that the lake waters were relatively low in sulfate (Figure 7). All the samples fall well below the ratio of organic carbon to pyrite sulfur contents of 2.8 that is typical of reducing marine sediments deposited under sulfate-replete conditions (Berner et al., 1979). In these sediments, microbial sulfate reduction and subsequent pyrite formation are limited by the diffusion of sulfate into the sedimentary pore waters. In contrast, euxinic sediment (deposited under anoxic, and hydrogen sulfide containing water columns) have C/S that fall plot above this 2.8 threshold and are instead limited by availability of highly reactive iron provided by the iron shuttle (Raiswell and Berner, 1985). Sediments deposited in sulfate-poor systems, such as lakes and freshwater wetlands, plot below the 2.8 line where microbial sulfate reduction and pyrite formation are limited by the overall availability of

sulfate (Berner and Raiswell, 1984). Together, the elevated Fe_{HR}/Fe_T and low Fe_{py}/Fe_{HR} and organic carbon-to-pyrite sulfur ratios indicate that deposition of the Cow Branch sediments was under anoxic, iron-rich (ferruginous) waters (Figures 2, 4, and 6).

The interpretation that lithofacies like 5a and 5b were deposited under an anoxic water column is consistent with the traditional deep water interpretation for these units (Arthur et al., 1984; Calvert et al., 1996) and agrees with hypothesis of depositional environments by Olsen (1986). Presence of laminations and elevated TOC content also suggest that they were below wave influence under a stratified water column. However it should be noted that the laminations can be biologically mediated (i.e. laminations created by benthic microbial mats), which may be the case for the wavy lamination (lithofacies 5a and 5b). This however does not refute the interpretation of a deep-water environment as microbial mats can be found both above and below chemoclines in modern environments. CITE

The presence of enriched Fe_{HR}/Fe_T that indicate anoxic, ferruginous conditions in lithofacies (1-4) that contain bioturbation and sedimentary structures indicative of current energy are in apparent conflict. However, these signals may point to intermittent anoxia, perhaps developing seasonally, where the substrate could have been colonized by benthic fauna at times, but the sediment retained the geochemical fingerprint of anoxia. Alternatively, these units may have been deposited at the base of the mixed layer, which at times allowed for presence of organisms, but still remained reducing (dysaerobic) enough for the iron shuttle to function and enrich the local highly reactive iron pool.

Overall, the iron speciation indicates that there was, indeed, at least intermittent and possibly persistent stratification of the water column based on enrichment of highly reactive iron throughout the cycle. This is further supported by the presence of high total

organic carbon contents through the middle portion of the section, including the insect layer. I suggest that those lithofacies (5-7) were persistently anoxic and were deposited during a lake transgression and high stand. Lithofacies near the top and bottom of the cycle (1-4) where the TOC is closer to background levels were probably intermittently anoxic or close enough to the chemocline to still enrich the highly reactive iron above fluvial Dry Fork levels.

3. Primary dolomite formation within the Dan River Basin

The iron carbonate is the primary host for the Fe_{HR} enrichment in the Cow Branch Formation (Figure 5) and dolomite is the dominant carbonate mineralogy throughout the formation (Table 1). In the context of the iron shuttle model this dolomite would have been formed syngenetically and/or during early diagenesis. This is in agreement with recent studies that suggest the majority of the microsparry dolomite within the Cow Branch is primary (Liutkus et al., 2010; Liutkus-Pierce et al., 2014).

Several models have been suggested for dolomite formation in lacustrine systems with high pH, high-Mg, and low salinity. These include primary precipitation of dolomicrite, the nodulization of dolomicrite, or local dissolution and replacement of Mg-rich clays during early diagenesis within the sediments (Casado et al., 2014). Additionally, dolomite precipitation in alkaline and saline lakes is thought to be mostly microbially mediated (Meister et al., 2011; DeDeckker and Last, 1989). The concurrence of dolomite within intervals with wavy laminations suggests a role for microbes in the formation of the Cow Branch dolomites. Given the lack of quartz in the Cow Branch Formation combined with the pseudosparry/microsparry dolomite associated with microbial laminites (Liutkus-Pierce et

al., 2014; Liutkus et al., 2010), it is likely that the dolomite within the basin is predominantly primary, and if that is the case, it provides evidence for an alkaline environment (Last, 1990). Carbonate accumulation in the alluvial formations of the Hartford basin, another East coast Mesozoic rift basin, has been noted and hypothesized as having resulted from a Ca-rich source rock, either from surface runoff or groundwater and precipitating due to the ephemeral paleolake dynamics (Gierlowski-Kordesch, 1998; Gierlowski-Kordesch and Rust, 1994). It follows that adjacent Paleozoic carbonates (King and Beikman, 1976) could have been a similar source to the Dan River Basin (Liutkus et al., 2010; Liutkus-Pierce et. al, 2014).

There is, as noted by Litukus et al. (2010; 2014), some secondary diagenetic dolomite overgrowths and coarsening an observation that I also note. Liutkus et al. (2010; 2014) observed that the dolomite cores are Ca-rich, while the secondary rims are predominantly Fe- and Mn-rich. However, Liutkus et al., (2010; 2014) consider the majority of dolomite to reflect syngenetic or early diagenetic dolomite due to: 1) the size of the microsparry dolomite crystals in the Cow Branch sediments (5–20 μm) which still fall within the range of biologically mediated, primary dolomite, 1–120 μm (Gierlowski- Kordesch 2010); 2) the preservation of distinct dolomite bearing laminae, and 3) the high porosity and permeability that would be needed for secondary dolomite precipitation. While I hypothesize here that the dissolution and subsequent coarsening of the dolomite was an early diagenetic process and the original highly reactive iron signature was preserved, the observation of coarser relatively Fe-rich rims and their implications for the iron speciation proxy warrants further investigation.

4. Organic carbon sources in the Dan River Basin

The relationship between the total organic carbon contents and their isotope composition from the Dan River Basin lithofacies can be used to infer the sources organic matter to the sediments the and processes that act on that organic matter (Meyers, 1994) In Figure 8, a cross plot of TOC content with $\delta^{13}C_{org}$, it is clear that lithofacies cluster together based on their interpreted depositional environment (i.e shallow lithofacies 1-4 and deeper lithofacies 5-7).

Lithofacies that are considered to be deep water (lithofacies 5-7) broadly tend to cluster along a vertical arm of the $\delta^{13}C_{org}$ versus TOC (Figure 8). They span a range of TOC values, but it is clear that they have a consistent and more negative $\delta^{13}C_{org}$ values than the shallower lithofacies (1-4). Given these observations the organic matter was likely sourced from primary production within the lake, coupled with a decreased input of terrigenous organic matter (Deines, 1980). The anoxic conditions within the deeper waters of the lake likely inhibited microbial degradation of the organic matter resulting in relatively higher TOC contents and preserving more negative $\delta^{13}C_{org}$ values (Deines, 1980; Talbot and Livingstone, 1989).

In contrast, lithofacies 1-4 cluster at lower TOC contents and have $\delta^{13}C_{org}$ span a range of values that are generally less negative relative to lithofacies 5-7 (Figure 8). Based on sedimentological observations these units were deposited under shallower waters under intermittently anoxic conditions. Since these lithofacies have a range of $\delta^{13}C_{org}$ values they may reflect the mixing of organic matter sources or the degraded organic matter, which drives $\delta^{13}C$ of organic matter to less negative values (Peterson and Fry, 1987). In order to

distinguish between these two hypotheses we compare the $\delta^{13}C_{org}$ of the lithofacies 1-4 of the Cow Branch to those of the Dry Fork Formation.

Organic matter in the Dry Fork Formation, since it is a fluvial unit, would be composed primarily of terrigenous organic matter. Organic matter from the Dry Fork Formation has slightly less negative $\delta^{13}C_{org}$ (~1‰) — as compared to the lithofacies 5-7 and the most negative values of lithofacies 1-4 of the Cow Branch (Figure 8). Therefore, mixing of this organic matter, of which degradation prior to deposition in the basin would only increase its $\delta^{13}C_{org}$ by 1-2‰ (Burchardt and Fritz, 1980) with that of primary production within the lake (i.e. $\delta^{13}C_{org}$ of lithofacies 5-7), cannot explain the full range of $\delta^{13}C_{org}$ values seen lithofacies 1-4. Thus, this suggests that the range of $\delta^{13}C_{org}$ seen in lithofacies 1-4 were caused by continual microbial degradation of organic matter during early diagenesis. This makes sense in the context of the low TOC contents of these units and the sedimentary observations that indicate the reworking of these units by bioturbation and current action; these processes would increase the oxygen exposure time of the organic mater aiding in its degradation.

5. Model for formation of the lagerstätten

Based on the data presented above, and in agreement with previous literature (Liutkus et al., 2010; Liutkus-Pierce et al., 2014; Olsen et al., 1989) deposition of the insect lagerstätte present in the studied cycle resides in an early to mid-lake transgression. The onset of the transgression is signaled by decreased sedimentation rates and a trend to finer-grained sediments. Bedding becomes gradually thinner until laminations dominate the transgressive and high-stand lithofacies (5-7). Sedimentary structures present in lithofacies below the lagerstätten, 1-4 and 8, like bioturbation, ripple cross-bedding and

scour marks signal an environment that was shallow and intermittently oxic enough to allow habitation by organisms.

The lagerstätte occurs in the interval right after the transition to the thin beds of lithofacies 5a that suggest a calmer and less marginal environment. The early part of this lithofacies transition also includes a short-lived spike in pyrite sulfur contents relative to both total iron and highly reactive iron, which I invoke to be the product of a slowing sedimentation rates, creating a condensed interval, often associated with transgression. The sulfur spike occurs well into the onset of the increase and subsequent long-term enrichment in total organic carbon, which suggests a transition of the depositional environment to a more persistently anoxic water column in a deeper-basinal setting.

The deposition of the lagerstätte was presumably the product of a combination of several environmental factors. The transgression of the lake was likely very important. In the initial phase of deepening of the lake, the source of the insects and other organisms, the shallow lake waters and lake margins, would have been relatively close to the spatial location of the lagerstätten's deposition, while the water column at the site of deposition was deep enough to maintain persistent benthic anoxia. The anoxic and potentially alkaline lake water chemistry at the site of fossil deposition inhibited scavenging of insects and other organisms below the chemocline. The ferruginous conditions within the lake also played role in the soft body preservation; a model for organic preservation has invoked a role of the adsorption of Fe(II) organic biomolecules as protecting organic fossil remains from decomposition by microbial enzymes (Petrovich, 2001). Thus, the unique chemistry of the lake combined with right depositional setting and position within the lake resulted in the formation of the lagerstätten-bearing interval.

E. Conclusions

The integration of sedimentological and geochemical data presented here point to deposition of the Triassic lagerstätte under anoxic, ferruginous and alkaline conditions during the initial phase of lake transgression. The relatively short time scale of lake level change is illustrated by lithofacies and geochemical progression in three stages. Stage 1 is composed of more marginal lithofacies 1-4 and broadly fines up towards Stage 2 (Figure 9A). Stage 2 is considered to be a more basinward depositional environment or lake high-stand, where the finest grained lithofacies are deposited and anoxia is persistent. Stage 2 includes the insect lagerstätten (Figure 9B). Stage 3 is the subsequent shoaling of the deep lake to more marginal sediments (Figure 9C). The shallow, half-graben style of the rift basin allowed for rapid change of lake level by orbital driven climate cycles. The predominantly dolomite- and analcime-rich mineralogy suggests that lake chemistry was alkaline through the majority of the cycle. Enrichment of the highly reactive iron pool in the Cow Branch Formation relative to the fluvial Dry Fork Formation points at least intermittent anoxic conditions throughout the cycle. In the context of the lagerstätten, these conditions may have eliminated or limited scavenging of the fossils. However the lake appears to have been sulfate-poor and never developed euxinia. The deposition and preservation of the lagerstätte was therefore likely a product of a goldilocks scenario within the cycle, where these spatial, sedimentological, and geochemical factors worked together to produce a world-class insect site.

F. References

Ackerman, R.V., Schlische, R.W., Patino, L.C., Johnson, L.A., 2003. A Lagerstatte of Rift-Related Tectonic Structures from the Solite Quarry, Dan River–Danville Rift Basin, in: Le-Tourneau, P.M., Olsen, P.E. (Eds.), The Great Rift Valleys of Pangea. Columbia University Press, pp. 118–133.

Aller, R.C., Mackin, J.E., Cox Jr, R.T., 1986. Diagenesis of Fe and S in Amazon inner shelf muds: apparent dominance of Fe reduction and implications for the genesis of ironstones. Cont. Shelf Res., Sedimentary Processes on the Amazon Continental Shelf 6, 263–289. doi:10.1016/0278-4343(86)90064-6

Arthur, M.A., Dean, W.E., Stow, D. a. V., 1984. Models for the deposition of Mesozoic-Cenozoic fine-grained organic-carbon-rich sediment in the deep sea. Geol. Soc. Lond. Spec. Publ. 15, 527–560. doi:10.1144/GSL.SP.1984.015.01.34

Berner, R.A., Baldwin, T., Holdren, G.R., 1979. Authigenic iron sulfides as paleosalinity indicators. J. Sediment. Res. 49, 1345–1350. doi:10.1306/212F7923-2B24-11D7-8648000102C1865D

Berner, R.A., Raiswell, R., 1984. C/S method for distinguishing freshwater from marine sedimentary rocks. Geology 12, 365–368. doi:10.1130/0091-7613(1984)12<365:CMFDFF>2.0.CO;2

Burchardt, B., Fritz, P., 1980. Environmental isotopes as environmental and climatological indicators, in: Fritz, P., Fontes, J.C. (Eds.), Handbook of Environmental Isotope Geochemistry. Elsevier, Amsterdam, pp. 473–504.

Calvert, S.E., Bustin, R.M., Ingall, E.D., 1996. Influence of water column anoxia and sediment supply on the burial and preservation of organic carbon in marine shales. Geochim. Cosmochim. Acta 60, 1577–1593. doi:10.1016/0016-7037(96)00041-5

Calvo, J.P., Rodriguez-Pascua, M., Martin-Velazquez, S., Jimenez, S., Vicente, G.D., 1998. Microdeformation of lacustrine laminite sequences from Late Miocene formations of SE Spain: an interpretation of loop bedding. Sedimentology 45, 279–292. doi:10.1046/j.1365-3091.1998.00145.x

Canfield, D.E., Poulton, S.W., Knoll, A.H., Narbonne, G.M., Ross, G., Goldberg, T., Strauss, H., 2008. Ferruginous Conditions Dominated Later Neoproterozoic Deep-Water Chemistry. Science 321, 949–952. doi:10.1126/science.1154499

Canfield, D.E., Raiswell, R., Westrich, J.T., Reaves, C.M., Berner, R.A., 1986. The use of chromium reduction in the analysis of reduced inorganic sulfur in sediments and shales. Chem. Geol. 54, 149–155. doi:10.1016/0009-2541(86)90078-1

Casado, A.I., Alonso-Zarza, A.M., La Iglesia, Á., 2014. Morphology and origin of dolomite in paleosols and lacustrine sequences. Examples from the Miocene of the Madrid Basin. Sediment. Geol. 312, 50–62. doi:10.1016/j.sedgeo.2014.07.005

Deines, P., 1980. The isotopic composition of reduced organic carbon, in: Fritz, P., Fontes, J.C. (Eds.), Handbook of Environmental Isotope Geochemistry. Elsevier, Amsterdam, pp. 329–406.

Farrell, U.C., Briggs, D.E.G., Hammarlund, E.U., Sperling, E.A., Gaines, R.R., 2013. Paleoredox and pyritization of soft-bodied fossils in the Ordovician Frankfort Shale of New York. Am. J. Sci. 313, 452–489. doi:10.2475/05.2013.02

Fraser, N.C., Grimaldi, D.A., Olsen, P.E., Axsmith, B., 1996. A Triassic lagerstatte from eastern North America. Nature 380, 615.
Froelich, A.J., Olsen, P.E., 1983. Newark Supergroup, a revision of the Newark Group in eastern North America. US Geol. Surv. Bull., Stratigraphic Notes 1537–A, A55–A58.
Gierlowski-Kordesch, E.H., 1998. Carbonate deposition in an ephemeral siliciclastic alluvial system: Jurassic Shuttle Meadow Formation, Newark Supergroup, Hartford Basin, USA. Palaeogeogr. Palaeoclimatol. Palaeoecol. 140, 161–184. doi:10.1016/S0031-0182(98)00039-X
Gierlowski-Kordesch, E.H., Rust, B.R., 1994. The Jurassic East Berlin Formation, Hartford Basin, Newark Supergroup (Connecticut and Massachusetts): a saline lake-playa-alluvial plain system, in: Renaut, R.W., Last, W.M. (Eds.), Sedimentology and Geochemistry of Modern and Ancient Saline Lakes, SEPM Special Publication. pp. 249–265.
Hay, R.L., 1966. Zeolites and Zeolitic Reactions in Sedimentary Rocks. Geol. Soc. Am. Spec. Pap. 85, 1–122. doi:10.1130/SPE85-p1
Kent, D.V., Olsen, P.E., 1997. Paleomagnetism of Upper Triassic continental sedimentary rocks from the Dan River–Danville rift basin (eastern North America). Geol. Soc. Am. Bull. 109, 366–377. doi:10.1130/0016-7606(1997)109<0366:POUTCS>2.3.CO;2
King, P.B., Beikman, H.M., 1976. The Paleozoic and Mesozoic Rocks; A Discussion to Accompany the Geologic Map of the United States, in: Geologic Survey Professional Paper 903. United States Government Printing Office, Washington.
Last, W.M., 1990. Lacustrine dolomite-an overview of modern, Holocene, and Pleistocene occurrences. Earth-Sci. Rev. 221–263.
Leleu, S., Hartley, A.J., van Oosterhout, C., Kennan, L., Ruckwied, K., Gerdes, K., 2016. Structural, stratigraphic and sedimentological characterisation of a wide rift system: The Triassic rift system of the Central Atlantic Domain. Earth-Sci. Rev. doi:10.1016/j.earscirev.2016.03.008
Liutkus, C.M., Beard, J.S., Fraser, N.C., Ragland, P.C., 2010. Use of fine-scale stratigraphy and chemostratigraphy to evaluate conditions of deposition and preservation of a Triassic Lagerstätte, south-central Virginia. J. Paleolimnol. 44, 645–666. doi:10.1007/s10933-010-9445-1
Liutkus-Pierce, C.M., Fraser, N.C., Heckert, A.B., 2014. Stratigraphy, sedimentology, and paleontology of the Upper Triassic Solite Quarry, North Carolina and Virginia. Elev. Geosci. Southeast. U. S. New Ideas Old Terranes—Field Guid. GSA Southeast. Sect. Meet. Blacksbg. Va. 2014 Geol. Soc. Am. Field Guide 35 255–269.
Lyons, T.W., Severmann, S., 2006. A critical look at iron paleoredox proxies: New insights from modern euxinic marine basins. Geochim. Cosmochim. Acta, A Special Issue Dedicated to Robert A. Berner 70, 5698–5722. doi:10.1016/j.gca.2006.08.021
McBride, J.H., 1991. Constraints on the structure and tectonic development of the Early Mesozoic South Georgia Rift, southeastern United States; Seismic reflection data processing and interpretation. Tectonics 10, 1065–1083. doi:10.1029/90TC02682
Meister, P., Reyes, C., Beaumont, W., Rincon, M., Collins, L., Berelson, W., Stott, L., Corsetti, F., Nealson, K.H., 2011. Calcium and magnesium-limited dolomite precipitation at Deep Springs Lake, California. Sedimentology 58, 1810–1830. doi:10.1111/j.1365-3091.2011.01240.x

Meyers, P.A., 1994. Preservation of elemental and isotopic source identification of sedimentary organic matter. Chem. Geol. 114, 289–302. doi:10.1016/0009-2541(94)90059-0
Olsen, P.E., 1986. A 40-Million-Year Lake Record of Early Mesozoic Orbital Climatic Forcing. Science 234, 842–848.
Olsen, P.E., Froelich, A.J., Daniels, D.L., Smoot, J.P., Gore, P.J.W., 1991. Rift basins of early Mesozoic age. Horton W Ed Geol. Carol. 142–170.
Olsen, P.E., Kent, D.V., Cornet, B., Witte, W.K., Schlische, R.W., 1996. High-resolution stratigraphy of the Newark rift basin (early Mesozoic, eastern North America). Geol. Soc. Am. Bull. 108, 40–77. doi:10.1130/0016-7606(1996)108<0040:HRSOTN>2.3.CO;2
Olsen, P.E., Reid, J.C., Taylor, K.B., Whiteside, J.H., Kent, D.V., 2015. Revised Stratigrahphy of Late Triassic Age Strata of the Dan River Basin (Virginia and North Carolina, USA) Based on Drill Core and Outcrop Data. Southeast. Geol. 51, 1–31.
Olsen, P.E., Remington, C.L., Cornet, B., Thomson, K.S., 1978. Cyclic Change in Late Triassic Lacustrine Communities. Science 201, 729–733.
Peterson, B.J., Fry, B., 1987. Stable Isotopes in Ecosystem Studies. Annu. Rev. Ecol. Syst. 18, 293–320.
Petrovich, R., 2001. Mechanisms of Fossilization of the Soft-Bodied and Lightly Armored Faunas of the Burgess Shale and of Some Other Classical Localities. Am. J. Sci. 301, 683–726. doi:10.2475/ajs.301.8.683
Poulton, S.W., Canfield, D.E., 2005. Development of a sequential extraction procedure for iron: implications for iron partitioning in continentally derived particulates. Chem. Geol. 214, 209–221. doi:10.1016/j.chemgeo.2004.09.003
Pratt, B.R., 1998. Molar-tooth structure in Proterozoic carbonate rocks: Origin from synsedimentary earthquakes, and implications for the nature and evolution of basins and marine sediment. GSA Bull. 110, 1028–1045. doi:10.1130/0016-7606(1998)110<1028:MTSIPC>2.3.CO;2
Raiswell, R., Anderson, T.F., 2005. Reactive iron enrichment in sediments deposited beneath euxinic bottom waters: constraints on supply by shelf recycling. Geol. Soc. Lond. Spec. Publ. 248, 179–194. doi:10.1144/GSL.SP.2005.248.01.10
Raiswell, R., Berner, R.A., 1985. Pyrite formation in euxinic and semi-euxinic sediments. Am. J. Sci. 285, 710–724. doi:10.2475/ajs.285.8.710
Raiswell, R., Buckley, F., Berner, R.A., Anderson, T.F., 1988. Degree of pyritization of iron as a paleoenvironmental indicator of bottom-water oxygenation. J. Sediment. Res. 58, 812–819. doi:10.1306/212F8E72-2B24-11D7-8648000102C1865D
Raiswell, R., Newton, R., Wignall, P.B., 2001. An Indicator of Water-Column Anoxia: Resolution of Biofacies Variations in the Kimmeridge Clay (Upper Jurassic, U.K.). J. Sediment. Res. 71, 286–294. doi:10.1306/070300710286
Raiswell, R., Reinhard, C.T., Derkowski, A., Owens, J., Bottrell, S.H., Anbar, A.D., Lyons, T.W., 2011. Formation of syngenetic and early diagenetic iron minerals in the late Archean Mt. McRae Shale, Hamersley Basin, Australia: New insights on the patterns, controls and paleoenvironmental implications of authigenic mineral formation. Geochim. Cosmochim. Acta 75, 1072–1087. doi:10.1016/j.gca.2010.11.013
Rodríguez-Pascua, M.A., Calvo, J.P., De Vicente, G., Gómez-Gras, D., 2000. Soft-sediment deformation structures interpreted as seismites in lacustrine sediments of the

Prebetic Zone, SE Spain, and their potential use as indicators of earthquake magnitudes during the Late Miocene. Sediment. Geol. 135, 117–135. doi:10.1016/S0037-0738(00)00067-1
Severmann, S., Lyons, T.W., Anbar, A., McManus, J., Gordon, G., 2008. Modern iron isotope perspective on the benthic iron shuttle and the redox evolution of ancient oceans. Geology 36, 487–490. doi:10.1130/G24670A.1
Smoot, J.P., 1991. Sedimentary facies and depositional environments of early Mesozoic Newark Supergroup basins, eastern North America. Palaeogeogr. Palaeoclimatol. Palaeoecol., Paleoenvironments of Salt Lakes 84, 369–423. doi:10.1016/0031-0182(91)90055-V
Stookey, L.L., 1970. Ferrozine---a new spectrophotometric reagent for iron. Anal. Chem. 42, 779–781. doi:10.1021/ac60289a016
Talbot, M.R., Livingstone, D.A., 1989. The Phanerozoic Record of Lacustrine Basins and Their Environmental Hydrogen index and carbon isotopes of lacustrine organic matter as lake level indicators. Palaeogeogr. Palaeoclimatol. Palaeoecol. 70, 121–137. doi:10.1016/0031-0182(89)90084-9
Van Houten, F.B., 1962. Cyclic sedimentation and the origin of analcime-rich Upper Triassic Lockatong Formation, west-central New Jersey and adjacent Pennsylvania. Am. J. Sci. 260, 561–576. doi:10.2475/ajs.260.8.561
Viollier, E., Inglett, P.W., Hunter, K., Roychoudhury, A.N., Van Cappellen, P., 2000. The ferrozine method revisited: Fe(II)/Fe(III) determination in natural waters. Appl. Geochem. 15, 785–790. doi:10.1016/S0883-2927(99)00097-9
Withjack, M.O., Schlische, R.W., Olsen, P.E., 1998. Diachronous Rifting, Drifting, and Inversion on the Passive Margin of Central Eastern North America: An Analog for Other Passive Margins. AAPG Bull. 82, 817–835.

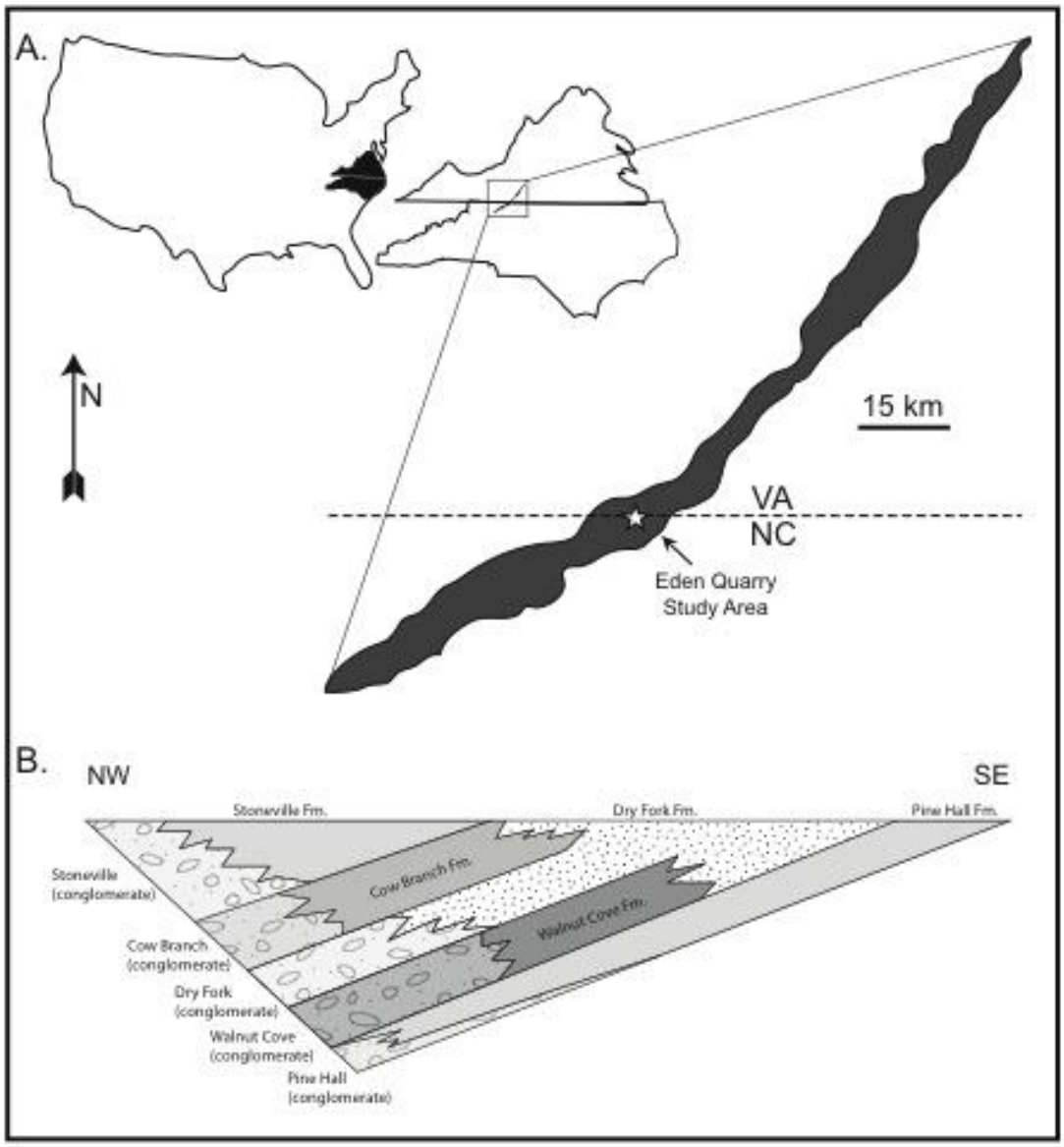

Figure 1 A.) Location map of Eden Quarry, Dan River Basin study area. Modified after Lyons and Severmann, 2006; Raiswell and Anderson, 2005 B.) Idealized stratigraphic cross-section of Dan River Basin fill modified after Olsen et al. (2015).

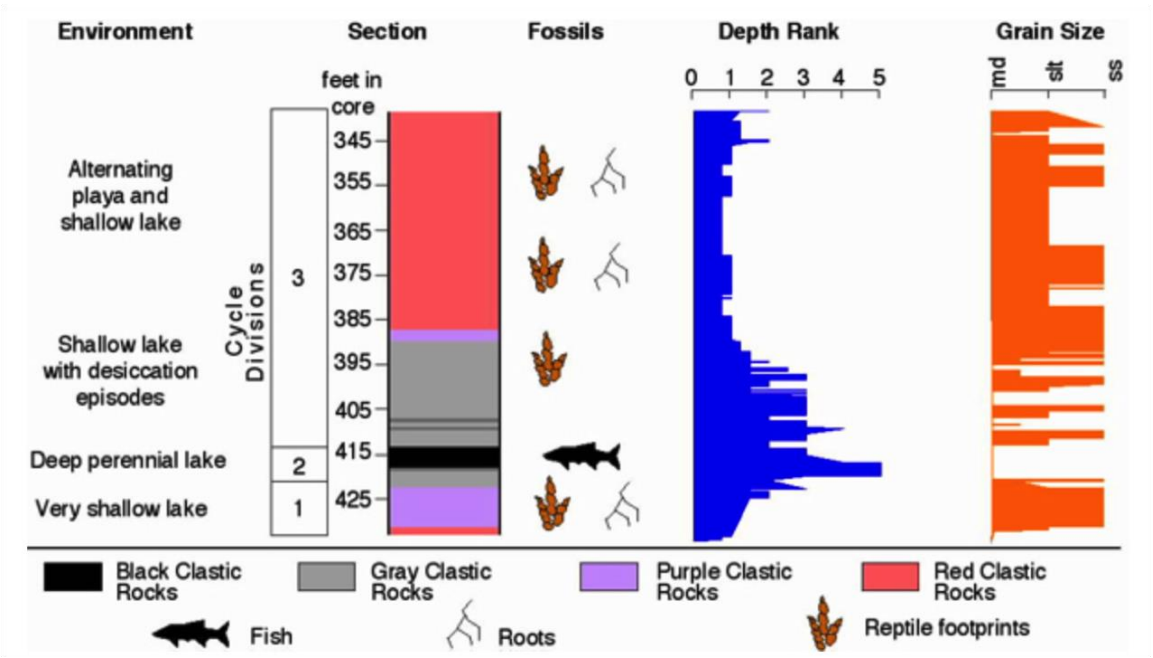

Figure 2 Idealized Van Houten Cycle for the Newark Basin, NJ. In the studied cycle within the Cow Branch Formation, no red clastic rocks are visible. Figure modified by Schlische, after Olsen et al., 1996.

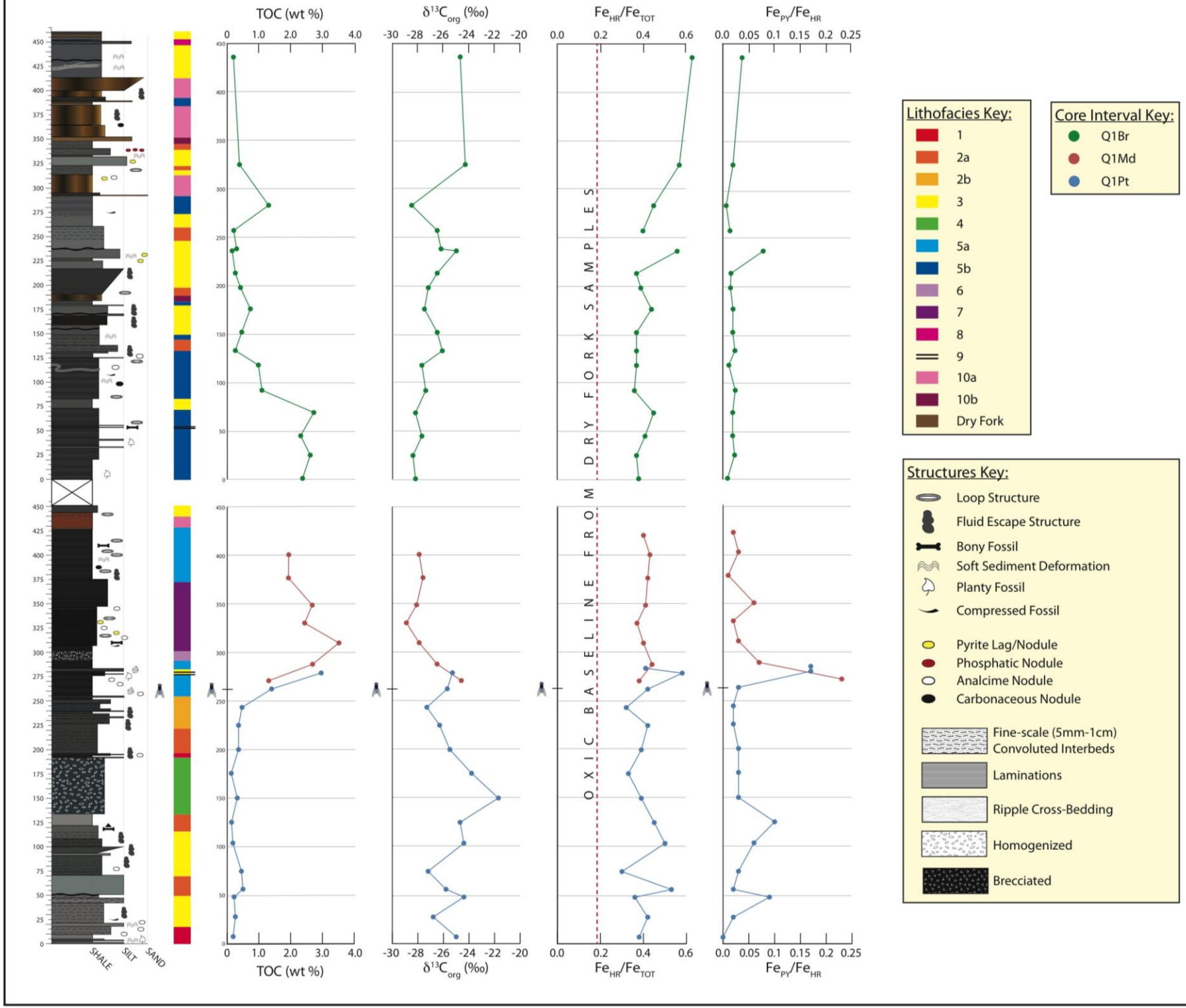
TOC (wt %)
δ13Corg (‰)
FeHR/FeTOT
FePY/FeHR
DRY FORK SAMPLES
OXIC BASELINE FROM
SHALE
SILT
SAND
Lithofacies Key:
1
2a
2b
3
4
5a
5b
6
7
8
9
10a
10b
Dry Fork
Core Interval Key:
Q1Br
Q1Md
Q1Pt
Structures Key:
Loop Structure
Fluid Escape Structure
Bony Fossil
Soft Sediment Deformation
Planty Fossil
Compressed Fossil
Pyrite Lag/Nodule
Phosphatic Nodule
Analcime Nodule
Carbonaceous Nodule
Fine-scale (5mm-1cm) Convoluted Interbeds
Laminations
Ripple Cross-Bedding
Homogenized
Brecciated

Figure 3 Stratigraphic column, lithofacies designations, and geochemistry of the studied succession of the Cow Branch Formation at the Eden Quarry**.** Geochemical data includes total organic carbon (TOC), organic carbon isotope data ($\delta^{13}C_{org}$), highly reactive iron to total iron ratio (Fe_{HR}/Fe_T), pyrite iron to highly reactive iron ratios (Fe_{py}/Fe_{HR}). Dry Fork baseline (average of all samples) is represented by the dotted red line on the Fe_{HR}/Fe_T plot.

Facies	Depth Int. (cm)	Type Thin Section	Lithologic Description	Geochemical Tendencies	Environmental Interpretation
1	B: 0-17 B: 192-196	Q1Pt-A (fig. 3.1)	Medium grey shale to fine silt interbedded with light grey to grey-blue fine to medium silt. Fine to medium silt beds included relatively coarse (medium sand) white grains, possibly analcime crystals. Interbeds are ~5mm scale and contacts are deformed by soft sediment deformation.	Low, background levels (< 0.25 wt%) of TOC, average $\delta^{13}C_{org}$ values. Background Fe_{HR}/Fe_{TOT} (0.4) and Fe_{PY}/Fe_{HR} (< 0.05) ratio.	Lake lowstand, near margins. Similar to Smoot (1991) facies L3
2a	B: 17-50 B: 116-134* B: 196-221 T: 132-144 T: 190-197 T: 246-260 T: 319-323 T: 340-345	Q1Pt-E (fig. 3.2)	Light to medium to dark grey shale to very fine silt with fine scale (approx. 1-5mm) convoluted interbeds. Intervals often contain “fluid escape structures” (or burrows) with occasional white (fine to medium sand size) grains. Appear to be bioturbated and somewhat homogenized. *Top of this interval begins to fine up and includes what we presume to be a fish bone or some vertebrate fossil.	Low, background levels (< 0.25 wt%) of TOC, average $\delta^{13}C_{org}$ values. Background Fe_{HR}/Fe_{TOT} (0.4) and Fe_{PY}/Fe_{HR} (< 0.05) ratio.	Lake lowstand, near margins. Similar to Smoot (1991) facies L3
2b	B: 221-255	Q1Pt-H (fig. 3.3)	Facies 2a and facies 3 interbedded at the 1-2 cm scale with irregular and/or deformed contacts.	Low, background levels (< 0.25 wt%) of TOC, trend towards lighter $\delta^{13}C_{org}$ values. Slightly lower than background Fe_{HR}/Fe_{TOT} and Fe_{PY}/Fe_{HR} ratio.	Lake lowstand, near margins. Similar to Smoot (1991) facies L3
3	B: 17-50 B: 70-116 B: 116-134 B: 276-282 B: 440-452 T: 71-83 T: 149-179 T: 197-245* T: 260-274 T: 314-319 T: 323-340* T: 413-446‡ T: 453-461	Q1Pt-C Q1Br-J (fig. 3.4)	Medium grey shale to fine silt, predominantly massive with some instances of mottled texture or soft sediment deformation based on color differences. These intervals are generally the coarsest facies that still remain grey in color. *These intervals include pyrite lags on the 3-5mm scale. The upper of the two starred intervals also include what we believe to be phosphatic nodules. ‡This interval includes a lighter grey blob, possibly an extrusion of another facies.	Low, background levels (< 0.25 wt%) of TOC, average $\delta^{13}C_{org}$ values. Background Fe_{HR}/Fe_{TOT} (0.4) and Fe_{PY}/Fe_{HR} (< 0.05) ratio.	Transitional facies, likely deposited during higher-order fluctuations from lowstand trending towards trangression and vice versa. Between Smoot (1991) facies L2 and L3
4	B: 134-192	Q1Pt-F (fig. 3.5)	Massive, homogenized unit, medium to dark grey, almost "slate blue". Generally composed of very fine silt with a heavy presence of medium sand sized white grains/crystals, visible to naked eye and with hand lens. Interval also includes medium to coarse silt sized black grains. Entirely bioturbated, no fining direction.	Low, background levels (< 0.25 wt%) of TOC, heaviest $\delta^{13}C_{org}$ values. Background Fe_{HR}/Fe_{TOT} (0.4) and Fe_{PY}/Fe_{HR} (< 0.05) ratio.	Marginal deposit with an abundance of benthic organisms to bioturbate section entirely. Similar to Smoot (1991) facies L2

Facies	Depth Int. (cm)	Type Thin Section	Lithologic Description	Geochemical Tendencies	Environmental Interpretation
5a	B: 255-276* B: 372-429	Q1Pt-J (fig. 3.6)	Very dark grey to black shale with very fine scale (sub-mm) laminations. Laminations are generally lighter than the black shale and are somewhat wavy in thin section. The intervals often contain coprolites within the bedding plane that create soft sediment deformation in areas. White grains of fine sand size are sometimes seen, but rare, as well as larger (medium-coarse sand) white nodules that appear to be made up of a number of smaller (coarse silt to fine sand size) white and black crystals. Compressed plant fossils are also occasionally visible. The higher of the two intervals includes what we presume to be bony fossil remnants as well as "loop structures" caused by microfaulting interrupting the fine scale laminations and creating the look of looped lamination structures. *This interval includes the insect layer.	Begin to trend to moderate to high values (1-3 wt%) of TOC, average $\delta^{13}C_{org}$ values. Highest Fe_{HR}/Fe_{TOT} (0.4-0.6) and Fe_{PY}/Fe_{HR} (0.05-0.25) ratio.	Lake transgression, transition from more marginal depositonal environment to deeper-basin. Still shallow enough to allow for some sediment reworking. Between Smoot (1991) facies L3 and L1
5b	T: 0-71 T: 83-132* T: 144-129 T: 179-184 T: 274-292 T: 384-393	Q1Br-E Q1Br-F (fig. 3.7)	Slightly coarser than facies 5, yet not a proper silt. Very dark grey to dark grey with similar fine scale (sub-mm) wavy laminations. Compressed plant fossils, preserved as silvery carbon images are visible on breakage planes parallel to bedding. Loop structures are observed in most intervals of this facies, under hand lens and in thin section. White grains as described previously are rare, but present, as well as previously described black grains. *This interval includes a lighter (medium grey) and somewhat coarser (very fine silt) structure that appears similar to the one seen in facies 3, possibly an extrusion of another facies.	Begin to trend to moderate to high values (1-3 wt%) of TOC, average $\delta^{13}C_{org}$ values. Background Fe_{HR}/Fe_{TOT} (0.4) and Fe_{PY}/Fe_{HR} (0.05) ratio.	Lake highstand, deeper-basinal deposition. Environment still allowed for growth of microbial mats Similar to Smoot (1991) facies L1
6	B: 292-301	No Thin Section Available	Black shale, almost coal-like to the touch. The interval is brecciated by a fault zone. No general breakage direction. Any fractures that are not entirely broken apart are filled with white calcite veins.	Not able to sample for specific geochemistry.	Fault zone, unable to be interpreted.

Facies	Depth Int. (cm)	Type Thin Section	Lithologic Description	Geochemical Tendencies	Environmental Interpretation
7	B: 301-372	No Thin Section Available	Very dark grey to black shale to very fine silt with approx. 2-5mm scale convoluted interbeds, noted by color change. The lower of the two intervals includes pyrite nodules on the mm scale, a presumed bony fossil as well as indistinguishable compressed fossils. Loop structures are also visible, though due to the dark color, they are often hard to pick out. Occasional white nodules and grains as described previously.	Highest values (2.5-3.5 wt%) of TOC, lightest $\delta^{13}C_{org}$ values. Background Fe_{HR}/Fe_{TOT} (0.4) and slightly elevated Fe_{PY}/Fe_{HR} (0.05-0.1) ratio.	Lake highstand. Deepest basinal facies present, probably below a chemocline. Similar to Smoot (1991) facies L1
8	T: 446-453	Q1Br-S (fig. 3.8)	Very dark grey shale to very fine silt that appears to show ripple cross bedding structures on the mm scale. The intervals are otherwise very similar to facies 7.	Not able to sample for specific geochemistry.	Lake lowstand, most marginal facies, sediment reworking by current. Similar to Smoot (1991) facies L2
9	B: 277.5 B: 280 T: 53.5 T: 55	Q1Pt-K (fig. 3.9)	Small scale (1-2mm) dark brown beds of fine silt. These beds occur in four isolated spots within the section. Used to correlate sections Pt and Md.	Not able to sample for specific geochemistry.	Interpreted to be times of increased carbonate deposition. Environment is otherwise similar to lithofacies they are located in. No Smoot (1991) likeness.
10a	B: 429-440 T: 292-314 T: 351-384 T: 393-413	Q1Br-N Q1Br-P (fig. 3.10)	Weathered units, ranging from medium brown to rust orange to light orange in color. Grain size ranges from borderline shale/very fine silt to fine sand. Fine sand intervals may be a product of dissolution of smaller grains and give the appearance of a larger grain size. Intervals are predominantly massive.	Weathered intervals - not sampled.	Weathered interval with no preserved structures, environmental interpretation not possible.
10b	T: 184-190 T: 345-351	Q1Br-M (fig. 3.11)	Same as facies 10 but with fine scale (sub mm) laminations still visible.	Weathered intervals - not sampled.	Weathered interval. Preserved laminations indicate deposition environment similar to Smoot (1991) facies L1

Table 1 Lithofacies designations, descriptions, type thin section examples, geochemical tendencies and broad environmental interpretation.

4.1

Lithofacies 1;

Cm-scale interbeds interrupted of ne silt and mud by soft sediment deformation and uid escape structures. Note the coarse-grained analcime.

4.2

Lithofacies 2a;

Homogenized section of ne-medium silt and ne sand sized grains. Note ning-up and presence of phosphatic fossil, as well as analcime.

4.3

Lithofacies 2b;

Lithofacies 2a and 3 interbedded on the 1-2 cm scale with contacts disrupted by soft sediment deformation.

4.4

a

b

Lithofacies 3;

Shale to ne silt with massive to mottled texture from soft sediment deformation.

Q1Br-J include pyrite lags towards the top of the thin section on the 3-5mm scale.

4.5

Lithofacies 4;

Entirely homogenized interval with an abundance of f ne-medium sand sized analcime grains.

4.6

Lithofacies 5a;

Finely laminated black shale. Thin section includes nodule/fossil creating soft sediment deformation.

4.7

a

b

Lithofacies 5b;

Finely laminated dark shale with an increased abundance of coarse silt-f ne sand analcime grains.

Q1Br-E includes nodule/fossil creating soft sediment deformation as well as microfaulting that results in loop structures in the laminations.

Q1Br-F includes an irregular intrusion of a f ner-grained, more carbonate-rich facies.

4.8

Lithofacies 8;

Interval is weathered, but represents a coarse silt with preserved structures of ripple cross-bedding and scour marks.

4.9

Lithofacies 9;

Thin section shows the set of browner, more carbonate-rich beds used to correlate core intervals Q1Pt and Q1Md to form the bottom core section.

4.10

a

b

Lithofacies 10a;

Thin sections show examples of weathered intervals that are predominantly massive but preserve some structures indicating homogenization or soft sediment deformation.

4.11

Lithofacies 10b;

Interval is weathered, but represents the preservation of f ne scale laminations.

Figure 4 Type thin sections of lithofacies.

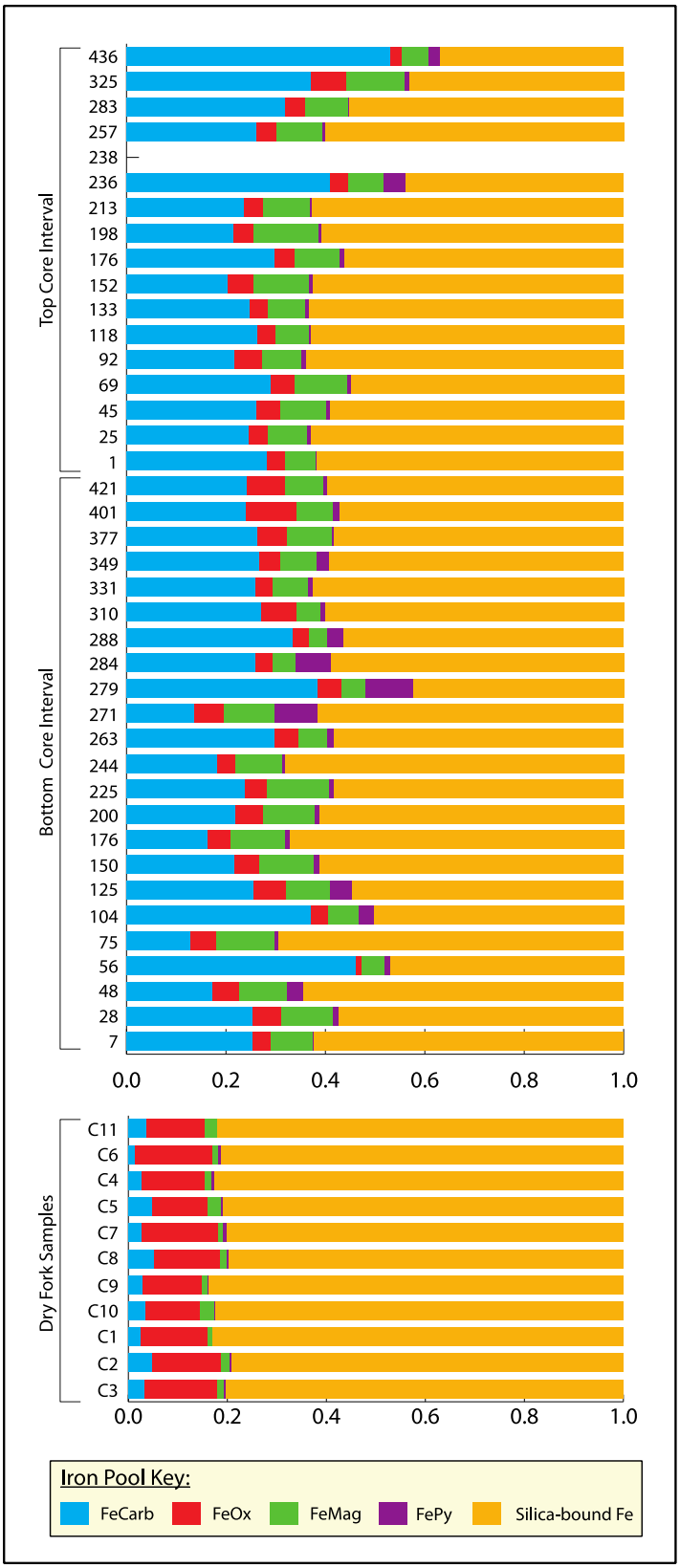

Figure 5 Bar graphs displaying the relative proportion of iron in the various iron-bearing phases for Cow Branch (at top) and Dry Fork samples (at the bottom). Note the higher proportion of highly reactive iron in the Cow Branch Formation samples versus the Dry Fork samples.

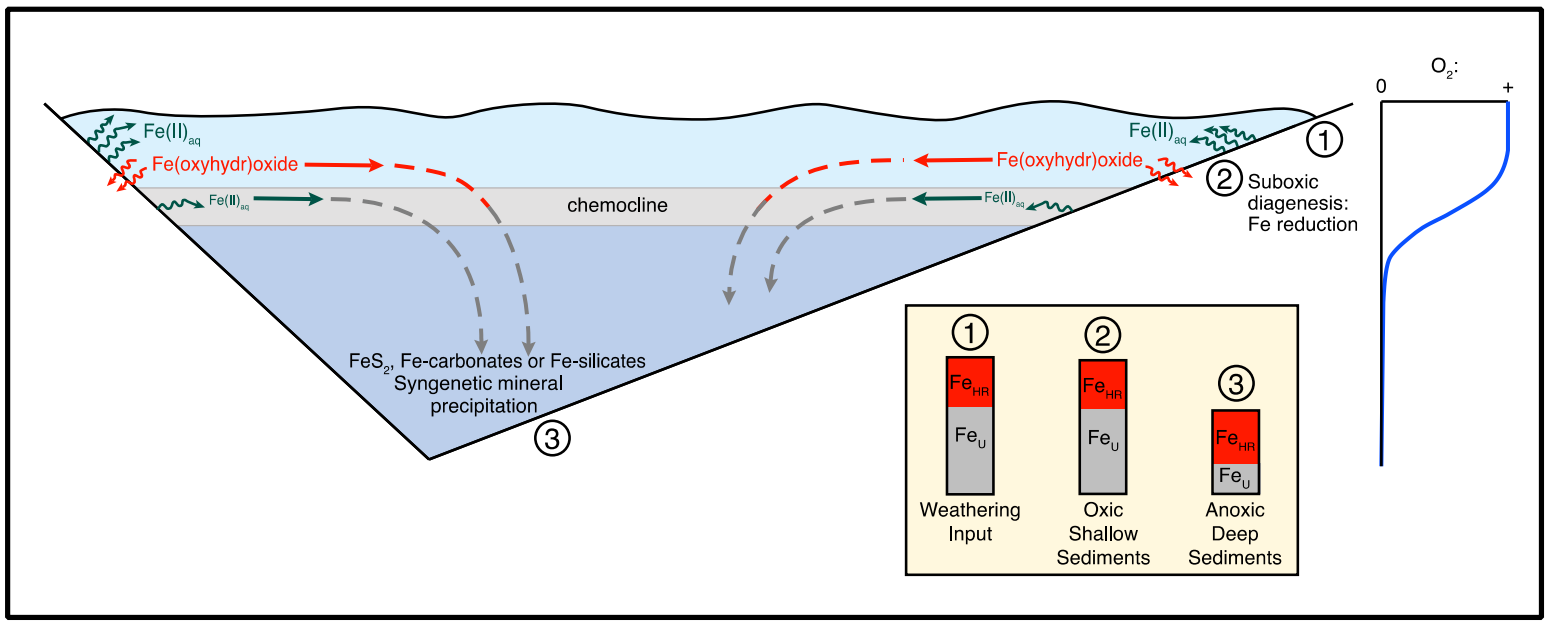

Figure 6 Idealized iron shuttle model for the Dan River Basin. After Severmann et al., 2008.

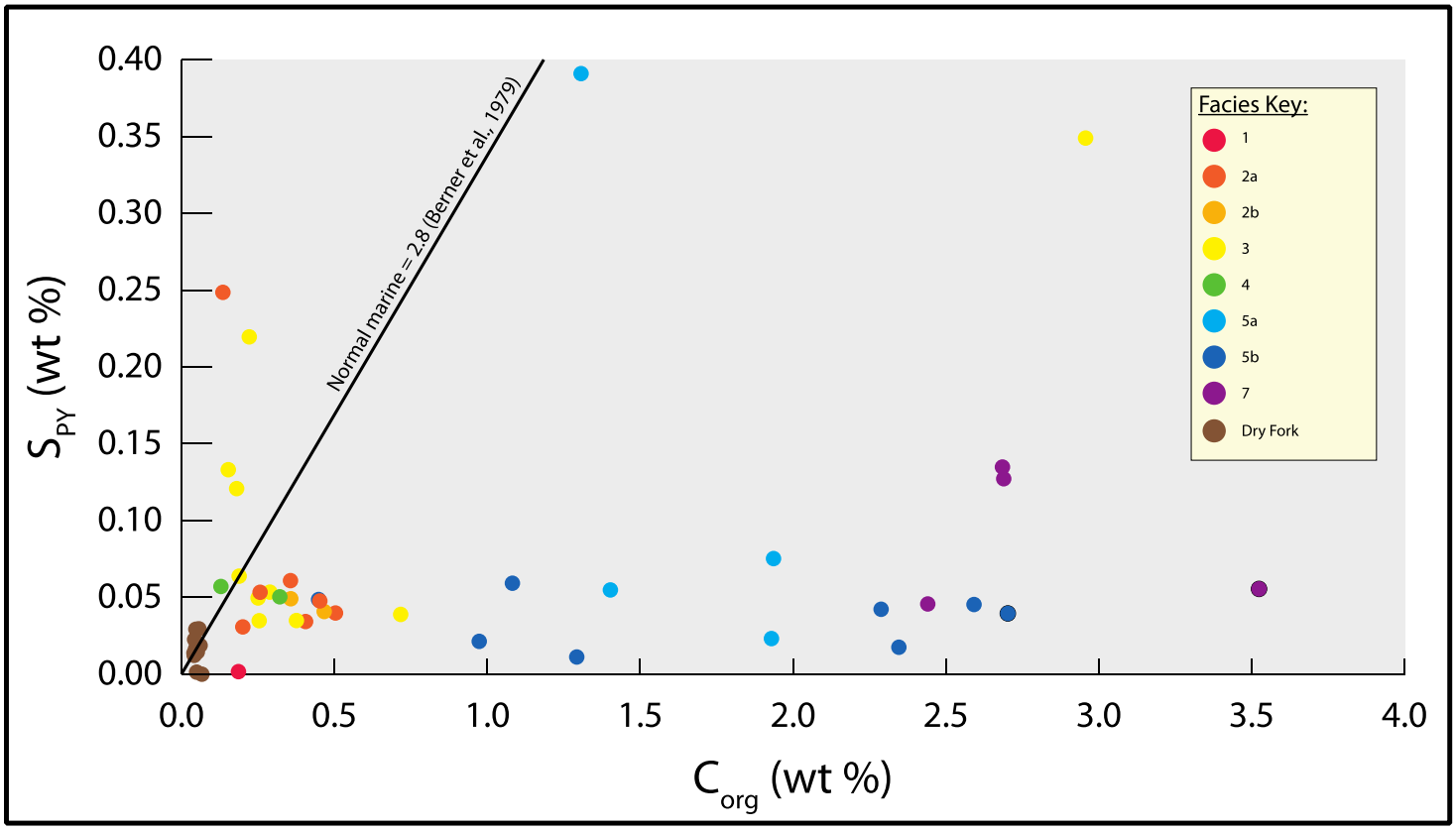

Figure 7 Organic carbon/pyrite sulfur plot, split by lithofacies designation. Most samples fall under the normal marine line (ratio of 2.8) from Berner et al., 1979.

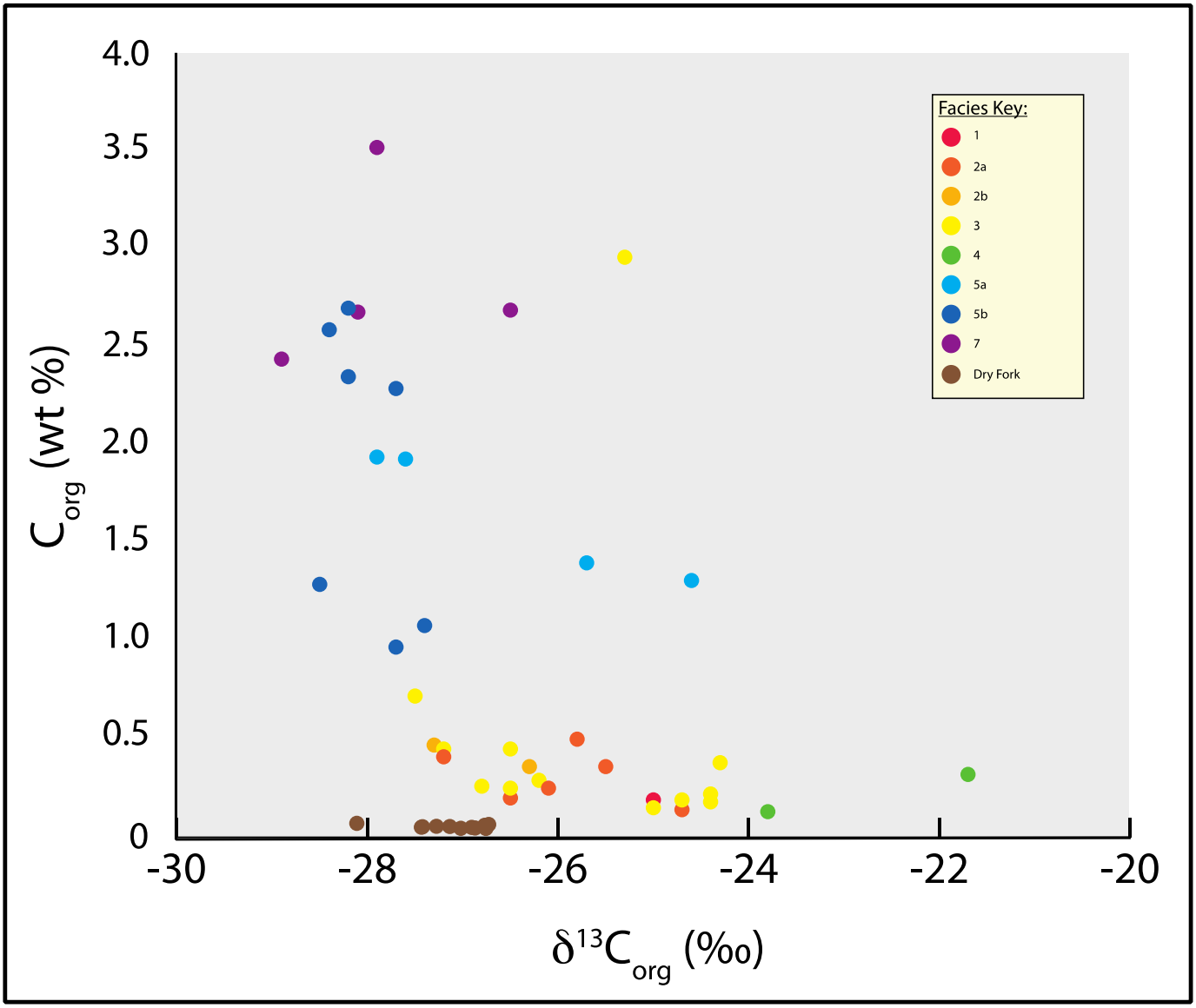

Figure 8 Organic carbon isotopes vs. organic carbon (wt %). Data are separated by lithofacies designation. Note the exponential decay trend with deeper facies on the vertical arm, and more shallow facies across the horizontal arm.

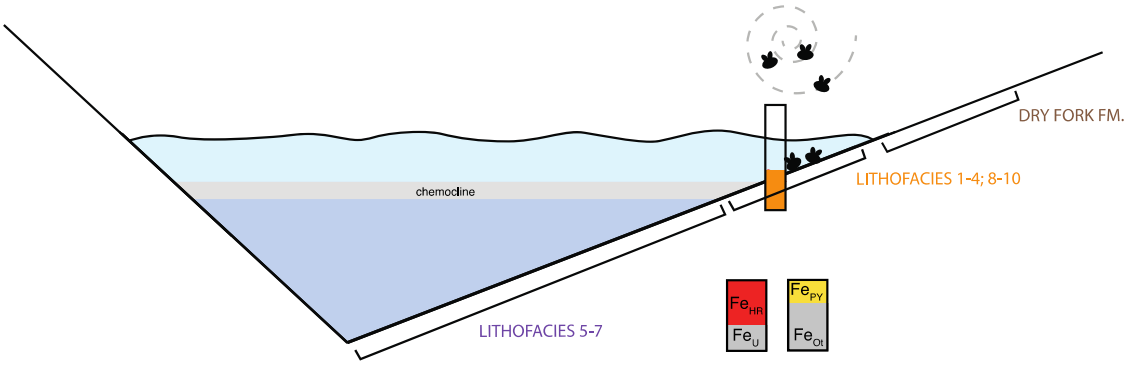

Figure 9A Stage 1 of cycle deposition. Marginal lithofacies are present and insect source is nearby. Depositional environment straddles the chemocline causing intermittent anoxia but preserving the geochemical signature.

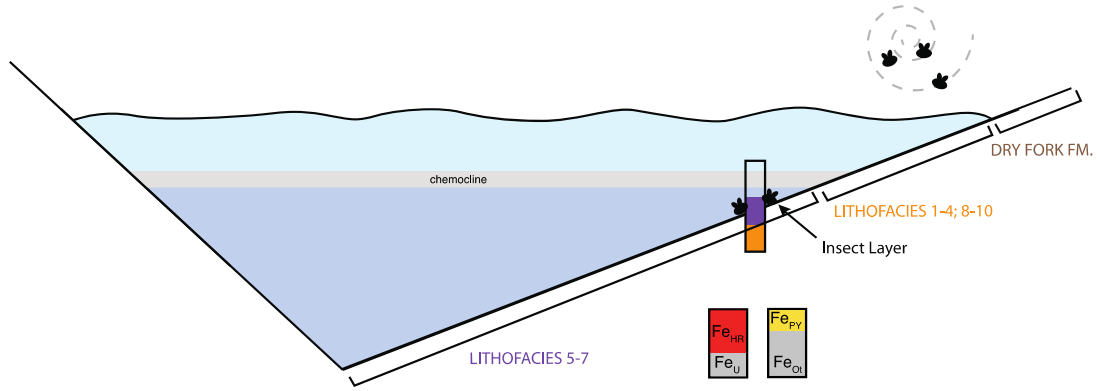

Figure 9B Stage 2 of cycle deposition, including the insect lagerstätte. Depositional environment becomes more basinward and chemocline transgresses creating a persistent anoxic environment. Lithofacies are indicative of lower energy and enriched in TOC.

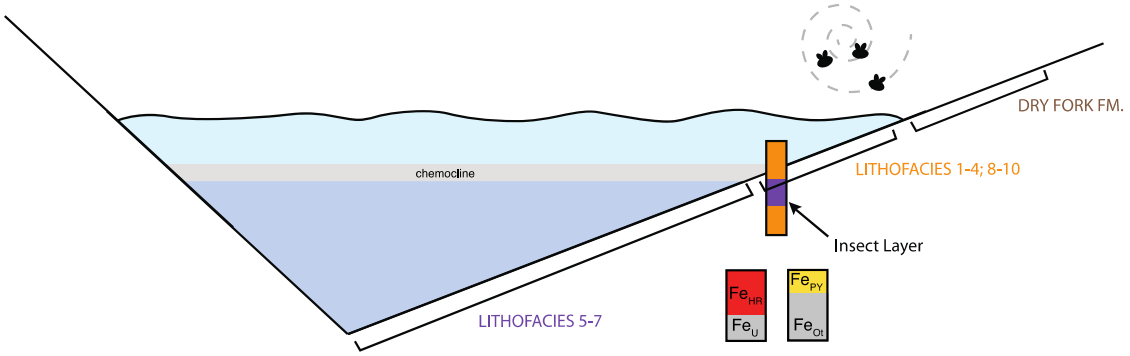

Figure 9C Stage 3 of cycle deposition. Shoaling of lake environment, again depositing marginal lithofacies in a broad coarsening up sequence. Geochemical signature of anoxia is preserved during intermittent anoxic conditions as depositional environment again straddles the chemocline.

Sample ID	Stratigraphic Order	Fe_T (wt%)	Fe_{carb} (wt%)	Fe_{ox} (wt%)	Fe_{mag} (wt%)	Fe_{Py} (wt%)	Fe_{HR} (wt%)	Fe_{HR}/Fe_T	Fe_{Py}/Fe_{HR}	S (wt%)	C (wt%)	δ13Corg (‰)
C3	11	5.47	0.18	0.80	0.07	0.02	1.07	0.20	0.02	0.02	0.061	-26.7
C2	10	4.04	0.19	0.57	0.07	0.01	0.84	0.21	0.02	0.01	0.052	-27.3
C1	9	4.78	0.12	0.65	0.04	0.00	0.81	0.17	0.00	0.00	0.067	-28.1
C10	8	6.24	0.21	0.69	0.17	0.02	1.09	0.17	0.01	0.02	0.046	-26.9
C9	7	4.94	0.14	0.60	0.05	0.01	0.80	0.16	0.02	0.01	0.041	-26.8
C8	6	3.95	0.20	0.53	0.05	0.01	0.80	0.20	0.01	0.01	0.042	-27.0
C7	5	4.15	0.11	0.64	0.05	0.03	0.82	0.20	0.04	0.03	0.057	-26.8
C5	4	4.67	0.22	0.53	0.12	0.02	0.89	0.19	0.02	0.02	0.051	-27.1
C4	3	4.20	0.11	0.53	0.06	0.02	0.73	0.17	0.03	0.02	0.043	-26.9
C6	2	4.95	0.06	0.77	0.06	0.03	0.92	0.19	0.03	0.03	0.047	-27.4
C11	1	6.45	0.23	0.77	0.15	0.00	1.15	0.18	0.00	0.00	0.050	-27.4

Sample ID	δ13Corg (‰)
Fossil Wood 1	-26.68
Fossil Wood 2	-26.04
Fossil Wood 3	-25.43
Fossil Wood 4	-25.46

Appendix A Data table for Dry Fork samples. Isotope data for fossil wood from the Cow Branch.
Appendix B Data table for Cow Branch Formation samples.

Sample' ID	Depth' (cm)	'Fe$_T$'(wt%)	Fe$_{carb}$'(wt%)	Fe$_{ox}$'(wt%)	Fe$_{mag}$'(wt%)	Fe$_{Py}$'(wt'%)	Fe$_{HR}$'(wt%)	Fe$_{HR}$/Fe$_T$	Fe$_{Py}$/Fe$_{HR}$	S (wt%)	C (wt%)	d13Corg (‰)
Q1Br-1	436	2.49	1.32	0.06	0.13	0.06	1.57	0.63	0.04	0.06	0.19	-24.7
Q1Br-2	325	2.92	1.08	0.21	0.34	0.03	1.66	0.57	0.02	0.03	0.38	-24.3
Q1Br-3	283	4.08	1.30	0.17	0.35	0.01	1.82	0.45	0.01	0.01	1.29	-28.5
Q1Br-4	257	5.22	1.36	0.20	0.49	0.03	2.09	0.40	0.01	0.03	0.20	-26.5
Q1Br-5a	238	5.34				0.05				0.05	0.29	-26.2
Q1Br-5b	236	3.02	1.23	0.11	0.22	0.13	1.69	0.56	0.08	0.13	0.15	-25.0
Q1Br-6	213	5.55	1.31	0.21	0.52	0.03	2.07	0.37	0.02	0.03	0.25	-26.5
Q1Br-7	198	5.59	1.20	0.22	0.73	0.03	2.19	0.39	0.01	0.03	0.41	-27.2
Q1Br-8	176	4.57	1.36	0.19	0.41	0.04	2.00	0.44	0.02	0.04	0.72	-27.5
Q1Br-9	152	6.29	1.28	0.32	0.71	0.04	2.36	0.37	0.02	0.05	0.45	-26.5
Q1Br-10	133	5.35	1.33	0.19	0.40	0.05	1.96	0.37	0.02	0.05	0.25	-26.1
Q1Br-11	118	5.14	1.35	0.19	0.35	0.02	1.91	0.37	0.01	0.02	0.97	-27.7
Q1Br-12	92	6.34	1.37	0.36	0.50	0.05	2.28	0.36	0.02	0.06	1.08	-27.4
Q1Br-13	69	4.65	1.35	0.22	0.49	0.04	2.10	0.45	0.02	0.04	2.70	-28.2
Q1Br-14	45	5.08	1.32	0.24	0.48	0.04	2.08	0.41	0.02	0.04	2.29	-27.7
Q1Br-15	25	5.43	1.33	0.21	0.42	0.05	2.01	0.37	0.02	0.05	2.59	-28.4
Q1Br-16	1	4.87	1.37	0.18	0.30	0.02	1.86	0.38	0.01	0.02	2.35	-28.2

Sample' ID	Depth' (cm)	'Fe$_T$'(wt%)	Fe$_{carb}$'(wt%)	Fe$_{ox}$'(wt%)	Fe$_{mag}$'(wt%)	Fe$_{Py}$'(wt'%)	Fe$_{HR}$'(wt%)	Fe$_{HR}$/Fe$_T$	Fe$_{Py}$/Fe$_{HR}$	S (wt%)	C (wt%)	d13Corg (‰)
Q1Md-1	421	5.50	1.33	0.42	0.43	0.03	2.22	0.40	0.02	0.03		
Q1Md-2	401	5.59	1.34	0.57	0.41	0.07	2.39	0.43	0.03	0.08	1.94	-27.9
Q1Md-3	377	5.07	1.33	0.31	0.45	0.02	2.12	0.42	0.01	0.02	1.93	-27.6
Q1Md-4	349	5.01	1.33	0.21	0.37	0.12	2.04	0.41	0.06	0.13	2.68	-28.1
Q1Md-5	330.5	4.94	1.27	0.17	0.36	0.05	1.85	0.37	0.02	0.05	2.44	-28.9
Q1Md-6	310	4.52	1.22	0.31	0.22	0.05	1.81	0.40	0.03	0.06	3.52	-27.9
Q1Md-7	288	3.97	1.33	0.12	0.15	0.13	1.73	0.44	0.07	0.13	2.69	-26.5
Q1Pt-1a	284	4.56	1.18	0.16	0.21	0.32	1.88	0.41	0.17	0.32		
Q1Pt-1b	279	3.61	1.38	0.17	0.17	0.35	2.08	0.58	0.17	0.35	2.96	-25.3
Q1Md-8	271	4.14	0.56	0.25	0.42	0.36	1.59	0.38	0.23	0.39	1.31	-24.6
Q1Pt-2	262.5	4.51	1.34	0.22	0.26	0.05	1.87	0.42	0.03	0.05	1.40	-25.7
Q1Pt-3	243.5	5.99	1.08	0.23	0.56	0.04	1.91	0.32	0.02	0.04	0.47	-27.3
Q1Pt-4	225	5.33	1.26	0.24	0.66	0.05	2.22	0.42	0.02	0.05	0.36	-26.3
Q1Pt-5	200	5.71	1.25	0.31	0.60	0.06	2.22	0.39	0.03	0.06	0.36	-25.5
Q1Pt-6	175.5	5.36	0.87	0.26	0.58	0.06	1.76	0.33	0.03	0.06	0.13	-23.8
Q1Pt-7	150	4.49	0.97	0.23	0.49	0.05	1.74	0.39	0.03	0.05	0.32	-21.7
Q1Pt-8	125	5.05	1.29	0.32	0.45	0.23	2.29	0.45	0.10	0.25	0.14	-24.7
Q1Pt-9	103.5	3.64	1.35	0.12	0.23	0.11	1.81	0.50	0.06	0.12	0.18	-24.4
Q1Pt-10	74.5	5.97	0.76	0.31	0.70	0.05	1.82	0.30	0.03	0.05	0.45	-27.2
Q1Pt-11a	56	2.84	1.31	0.04	0.13	0.04	1.51	0.53	0.02	0.04	0.50	-25.8
Q1Pt-11b	48	5.97	1.03	0.32	0.57	0.20	2.12	0.36	0.09	0.22	0.22	-24.4
Q1Pt-12	27.5	5.33	1.35	0.31	0.56	0.05	2.26	0.42	0.02	0.05	0.26	-26.8
Q1Pt-13	7	5.40	1.37	0.19	0.46	0.00	2.03	0.38	0.00	0.00	0.19	-25.0